










DEAD-BOX RNA HELICASE 27 regulates microRNA biogenesis, zygote division, and stem cell homeostasis

Xiu-Li Hou ^{1,2}, Wen-Qiang Chen ^{1,2}, Yifeng Hou ³, Hua-Qin Gong ¹, Jing Sun ³, Zhen Wang ³, Heng Zhao ⁴, Xiaofeng Cao ^{2,3}, Xiu-Fen Song ^{1,2,*} and Chun-Ming Liu ^{1,2,4,*}

- 1 Key Laboratory of Plant Molecular Physiology, Institute of Botany, Chinese Academy of Sciences, Beijing 100093, China
- 2 College of Life Sciences, University of Chinese Academy of Sciences, Beijing 100049, China
- 3 State Key Laboratory of Plant Genomics and National Center for Plant Gene Research, CAS Center for Excellence in Molecular Plant Sciences, Institute of Genetics and Developmental Biology, Chinese Academy of Sciences, Beijing 100101, China
- 4 Institute of Crop Sciences, Chinese Academy of Agricultural Sciences, Beijing 100081, China

*Author for correspondence: xfsong@ibcas.ac.cn (X.-F.S.); cmliu@ibcas.ac.cn (C.-M.L.)

C.-M.L. designed and supervised the project. X.-L.H. performed most of the experiments. H.-Q.G. screened the mutant library and cloned the gene. W.-Q.C., Y.H., and Z.W. performed the biochemical experiments. J.S. analyzed the deep sequencing data. C.-M.L., X.-L.H., and X.-F.S. analyzed the data and wrote the manuscript. H.Z. and X.C. helped with revising the manuscript. All authors read and approved the manuscript.

The author responsible for distribution of materials integral to the findings presented in this article in accordance with the policy described in the Instructions for Authors (<https://academic.oup.com/plcell>) is: X.-F.S. (xfsong@ibcas.ac.cn) and C.-M.L. (cmliu@ibcas.ac.cn).

Abstract

After double fertilization, zygotic embryogenesis initiates a new life cycle, and stem cell homeostasis in the shoot apical meristem (SAM) and root apical meristem (RAM) allows plants to produce new tissues and organs continuously. Here, we report that mutations in *DEAD-BOX RNA HELICASE 27* (*RH27*) affect zygote division and stem cell homeostasis in *Arabidopsis* (*Arabidopsis thaliana*). The strong mutant allele *rh27-1* caused a zygote-lethal phenotype, while the weak mutant allele *rh27-2* led to minor defects in embryogenesis and severely compromised stem cell homeostasis in the SAM and RAM. *RH27* is expressed in embryos from the zygote stage, and in both the SAM and RAM, and *RH27* is a nucleus-localized protein. The expression levels of genes related to stem cell homeostasis were elevated in *rh27-2* plants, alongside down-regulation of their regulatory microRNAs (miRNAs). Further analyses of *rh27-2* plants revealed reduced levels of a large subset of miRNAs and their pri-miRNAs in shoot apices and root tips. In addition, biochemical studies showed that *RH27* associates with pri-miRNAs and interacts with miRNA-biogenesis components, including *DAWDLE*, *HYPONASTIC LEAVES 1*, and *SERRATE*. Therefore, we propose that *RH27* is a component of the microprocessor complex and is critical for zygote division and stem cell homeostasis.

Introduction

Zygote division is the initial step of embryogenesis in sexual organisms (Palovaara et al., 2016; Schulz and Harrison, 2019). In *Arabidopsis* (*Arabidopsis thaliana*), the zygote first elongates and then divides asymmetrically to produce a smaller apical cell and a larger basal cell. After two rounds of longitudinal divisions and one round of transverse division, the apical cell forms an eight-cell embryo. The embryo then undergoes periclinal

divisions that separate the outer protoderm and the inner ground tissue cells at the dermatogen stage. Later, the shoot apical meristem (SAM), root apical meristem (RAM), and two cotyledons are initiated from the globular staged embryo (Palovaara et al., 2016). Genetic studies have shown that mutations of *CULLIN1* (*CUL1*), *EMBRYONIC FACTOR 1* (*FAC1*), *CELL DIVISION CYCLE 5* (*CDC5*), *ZEUS1* (*ZEU1*), *DNA LIGASE 1* (*LIG1*), *YAOZHE* (*YAO*), *ZAK IXIK* (*ZIX*), *GAMETE CELL DEFECTIVE 1* (*GCD1*), *FAC19*, *ZYGOTE-ARREST 1* (*ZYG1*),

IN A NUTSHELL

Background: In higher plants, embryogenesis initiates from a zygote, followed by cell divisions and differentiation to form a mature embryo. During embryo development, stem cells in shoot apical meristem (SAM) and root apical meristem (RAM) are established; these stem cells allow plants to continuously generate new tissues and organs during post-embryonic growth. To date, about ten genes essential for zygote division have been reported, and transcription factors, peptide hormones and microRNAs (miRNAs) critical for stem cell homeostasis are known. DEAD-box RNA helicases regulate RNA metabolism such as mRNA export, mRNA splicing and rRNA processing, but whether they are involved in zygote division and stem cell homeostasis had remained elusive.

Question: We took a molecular genetic approach in Arabidopsis to identify genes that are essential for the initiation of zygote divisions and for the maintenance of stem cells in SAM and RAM.

Findings: We observed that *rh27-1*, a loss-of-function mutation of the *DEAD-box RNA helicase 27 (RH27)*, is zygote-lethal, and *rh27-2*, a partial loss-of-function mutation of the same gene, severely disrupted stem cell homeostasis in both the SAM and the RAM. *RH27* is expressed in the zygote and embryos during embryogenesis, and in shoot apices and root tips after seed germination. The abundances of several miRNAs related to stem cell homeostasis are reduced in shoot apices and root tips of *rh27-2*, and the expressions of their target genes are increased. Further analyses revealed that the levels of primary miRNAs (pri-miRNAs) also decreased in *rh27-2*. *RH27* is able to bind pri-miRNAs in vivo, and interacts with miRNA biogenesis components including DCL1, DDL, HYL1 and SE in nucleus, suggesting a critical role of *RH27* in zygote division, stem cell homeostasis and miRNA biogenesis.

Next steps: Further studies are needed to elucidate the role of miRNA in zygote division, and if a DEAD-box RNA helicase is a general component of miRNA biogenesis in plants.

or ZYG3 result in a zygote-lethal phenotype (Shen et al., 2002; Xu et al., 2005; Lin et al., 2007; Ronceret et al., 2008; Andreuzza et al., 2010; Li et al., 2010; Ngo et al., 2012; Wu et al., 2012; Yu et al., 2012; Guo et al., 2016; Yang et al., 2017), suggesting that these genes play a critical role in the initiation of zygote division.

Stem cells located in the SAM and RAM give rise to new tissues and organs continuously during post-embryonic development (Weigel and Jürgens, 2002). In Arabidopsis, the SAM is characterized by a convex structure that is divided into three zones: the central zone at the summit, the rib zone underneath, and the peripheral zone at the sides. Stem cells are located at the three outermost cell layers (L1–L3) in the central zone of the SAM, and the stem cell organizing center (SCOC) is located underneath and partially overlaps with the stem cell domain (Meyerowitz, 1997). A feedback regulatory loop, established via stem cell promotion by the homeodomain transcription factor WUSCHEL (WUS) and stem cell restriction by the CLAVATA3 (CLV3) peptide-CLV1/CLV2/CORYNE (CRN)/RECEPTOR-LIKE PROTEIN KINASE 2 (RPK2) receptors, maintains the homeostasis of stem cells in the SAM (Fletcher et al., 1999; Brand et al., 2000; Schoof et al., 2000; Müller et al., 2008; Kinoshita et al., 2010). HAIRY MERISTEM 1 (HAM1), a GRAS family transcription factor, acts as a co-factor of WUS to repress stem cell differentiation (Zhou et al., 2015). In the RAM, stem cells of different cell lineages are in direct contact with four rarely dividing cells termed the quiescent center (QC), which is the SCOC in the RAM (Dolan et al., 1993). Similar to the scenario in the SAM, WUSCHEL-RELATED HOMEODOMAIN 5 (WOX5) and CLV3/EMBRYO SURROUNDING REGION-RELATED 40 (CLE40) peptide-ARABIDOPSIS CRINKLY4 (ACR4)/CLV1

receptor kinase complexes form a feedback regulatory loop that controls distal stem cell homeostasis in the RAM (Stahl et al., 2009, 2013).

MicroRNAs (miRNAs) play a critical role in maintaining stem cell homeostasis in the SAM and RAM by down-regulating the expression of their target genes (Li et al., 2017). MiR171 represses the expression of *HAM1* (Llave et al., 2002), and ectopic expression of miR171-resistant *HAM1* in the L1 layer of the SAM leads to reduced expression of *CLV3*, and consequently an enlarged SAM (Zhou et al., 2018). MiR164 down-regulates the expression of *CUP-SHAPED COTYLEDON1 (CUC1)* and *CUC2*, which are involved in defining the organ boundary of the SAM (Mallory et al., 2004a). In the stele, miR165/166 restricts the expression of *PHABULOSA (PHB)*, which is critical for determination of the xylem cell fate in the RAM (Carlsbecker et al., 2010). In animals, miRNAs are generated through the cleavage and processing of primary miRNAs (pri-miRNAs) by Drosha, DGCG8, and Dicer (Grishok et al., 2001; Gregory et al., 2004). DEAD-box RNA helicases modulate the cleavage of pri-miRNAs by interacting with Drosha (Han et al., 2014; Yin et al., 2015; Zhao et al., 2016). In plants, miRNAs are generated by a microprocessor complex comprising DICER-LIKE 1 (DCL1), HYPONASTIC LEAVES 1 (HYL1), and SERRATE (SE; Wang et al., 2019b). In Arabidopsis, the DEAD-box RNA helicase family contains 58 members (Mingam et al., 2004), some of which are implicated in RNA processing events such as mRNA export, mRNA splicing, and rRNA processing (Gong et al., 2005; Liu et al., 2010; Guan et al., 2013; Paieri et al., 2018; Wang et al., 2019a). However, the role of DEAD-box RNA helicases in miRNA biogenesis has not been reported in plants.

In this study, we show that *DEAD-BOX RNA HELICASE 27* (*RH27*) is critical for zygote division and stem cell homeostasis in Arabidopsis. The strong mutant allele of *rh27-1* exhibited a zygote-lethal phenotype, while the weak allele of *rh27-2* exhibited compromised stem cell homeostasis in both the SAM and RAM. In *rh27-2* plants, the expression of several stem cell homeostasis-related genes, including *HAM1*, *CUC1*, *CUC2*, and *PHB*, was up-regulated, alongside reduced levels of miR171, miR164, and miR165/166. Small RNA sequencing (RNA-seq) showed reduced accumulation of a large subset of miRNAs in the *rh27-2* line. In addition, biochemical studies revealed that RH27 is associated with pri-miRNAs and interacts with DAWDLE (DDL) and the microprocessor complex components HYL1 and SE, suggesting that RH27 regulates miRNA biogenesis and is required for zygote division and stem cell homeostasis.

Results

The *zyg4-1* mutant with a point mutation in *RH27* exhibits a zygote-lethal phenotype

To identify genes that are essential for zygote division, a genetic screen was performed in an ethyl methanesulfonate-mutagenized M2 population of Arabidopsis, as described previously (Guo et al., 2016). This process enabled the identification of the zygote-lethal mutation *zygote-arrest 4-1* (*zyg4-1*). A genetic analysis showed that 26.1% of ovules ($n = 621$) produced in the heterozygous *zyg4-1/+* plants were aborted (Figure 1, A and Table 1), indicating that *zyg4-1* is inherited as a single-gene recessive mutation. Reciprocal crosses between *zyg4-1/+* and wild-type (Col-0) plants revealed that, when *zyg4-1/+* was used as the female, 96 of the 174 BC1 plants genotyped were wild type and 78 were heterozygous. This finding is consistent with the ratio of 1:1 (χ^2 test, $P = 0.17$), suggesting that the mutation of *zyg4-1* did not affect female gametogenesis. The same result was observed when *zyg4-1/+* was used as the pollen donor ($n = 347$, χ^2 test, $P = 0.63$), indicating that the mutation of *zyg4-1* did not affect male gametogenesis.

Whole-mount clearing of early staged ovules from *zyg4-1/+* plants, followed by Nomarski optical analyses, showed that 80.7% of the aborted embryos were arrested at the zygote stage, and the remainder were able to undergo one or two rounds of cell division ($n = 186$; Figure 1, B), indicating that ZYG4 is essential for zygote division.

Map-based cloning allowed us to localize the *zyg4-1* mutation to chromosome 5, and a G-to-A substitution in the coding region of At5g65900, which led to conversion of the tryptophan (W) 417 residue to a stop codon, was identified (Figure 1, C). At5g65900 encodes the DEAD-box RNA helicase RH27 (Aubourg et al., 1999), which contains all 12 conserved domains present in DEAD-box RNA helicase proteins (Supplemental Figure S1).

To test whether the mutation in RH27 was responsible for the observed zygote-lethal phenotype of *zyg4-1*, we generated a construct that carried the full-length genomic DNA of RH27, including the 2,227-bp upstream region, in-frame

fused to the coding sequence for the N-terminus of β -glucuronidase (GUS; *ProRH27:RH27-GUS*), and transformed it into wild-type Arabidopsis by *Agrobacterium tumefaciens*-mediated floral dip (Clough and Bent, 1998). Single-insertion homozygous *ProRH27:RH27-GUS* transgenic plants were then crossed with the *zyg4-1/+* line. Among the F2 population examined, heterozygous *zyg4-1/+* and homozygous *zyg4-1* plants carrying *ProRH27:RH27-GUS* (Supplemental Figure S2) showed no defects in embryogenesis (Figure 1, A) or post-embryonic development (Figure 1, D), indicating that *ProRH27:RH27-GUS* was able to completely rescue the zygote-lethal phenotype of *zyg4-1*. We thus renamed *zyg4-1* as *rh27-1*.

The weak mutant allele *rh27-2* shows minor defects in embryogenesis and severely compromised stem cell homeostasis in the SAM and RAM

To decipher the function of RH27, we obtained the *rh27-2* line, which carries a T-DNA insertion in the first exon of RH27 (SALK_068661, Figure 1, C), from the Arabidopsis Biological Resources Center. Heterozygous *rh27-2/+* plants grew normally during the vegetative phase, but 24.4% of the seeds produced in these plants were shriveled or wrinkled ($n = 1,625$; Figure 1, A; Supplemental Figure S3; and Table 1), indicating that *rh27-2* is a single-gene recessive mutant. Nomarski imaging at the time when the wild-type embryos were at the cotyledonary stage revealed that the embryos in the abnormal seeds from *rh27-2/+* plants were at the globular to bent cotyledon stages, suggesting a late embryo-defective phenotype (Figure 1, E). A germination test showed that 77.5% of these abnormal seeds were able to germinate ($n = 40$) and were genotyped to be homozygous for *rh27-2* (Figure 1, F). Whole-mount clearing of ovules at 3 days after pollination (DAP) revealed abnormal cell division patterns in *rh27-2* embryos from the 16-cell stage onward (Figure 1, G).

Compared with the wild-type seedlings, the *rh27-2* seedlings showed a short-root phenotype, with very slow growth of the primary roots (Figure 1, D and H). At the bolting stage, 58.9% of *rh27-2* plants showed a multi-shoot phenotype, with two or occasionally three shoots formed simultaneously ($n = 56$), compared with one formed in the wild-type plants ($n = 64$, Figure 1, I). Reciprocal crosses between *rh27-1/+* and *rh27-2/+* plants showed that approximately one-quarter of the ovules produced in F1 siliques were aborted (Table 1), confirming that *rh27-1* and *rh27-2* are allelic.

Reverse transcription PCR (RT-PCR) analyses of different regions of RH27 transcripts in *rh27-2* seedlings revealed that, although the full-length RH27 transcript was not detectable, transcripts upstream and downstream of the T-DNA insertion were detected (Figure 1, J). Since the insertion is located at the first exon of the gene, we speculated that it may have removed the non-conserved N-terminal region (Supplemental Figure S1), producing a truncated RH27 protein (Δ RH27) with partially compromised function. To test this hypothesis, a construct carrying the RH27 5'-regulatory

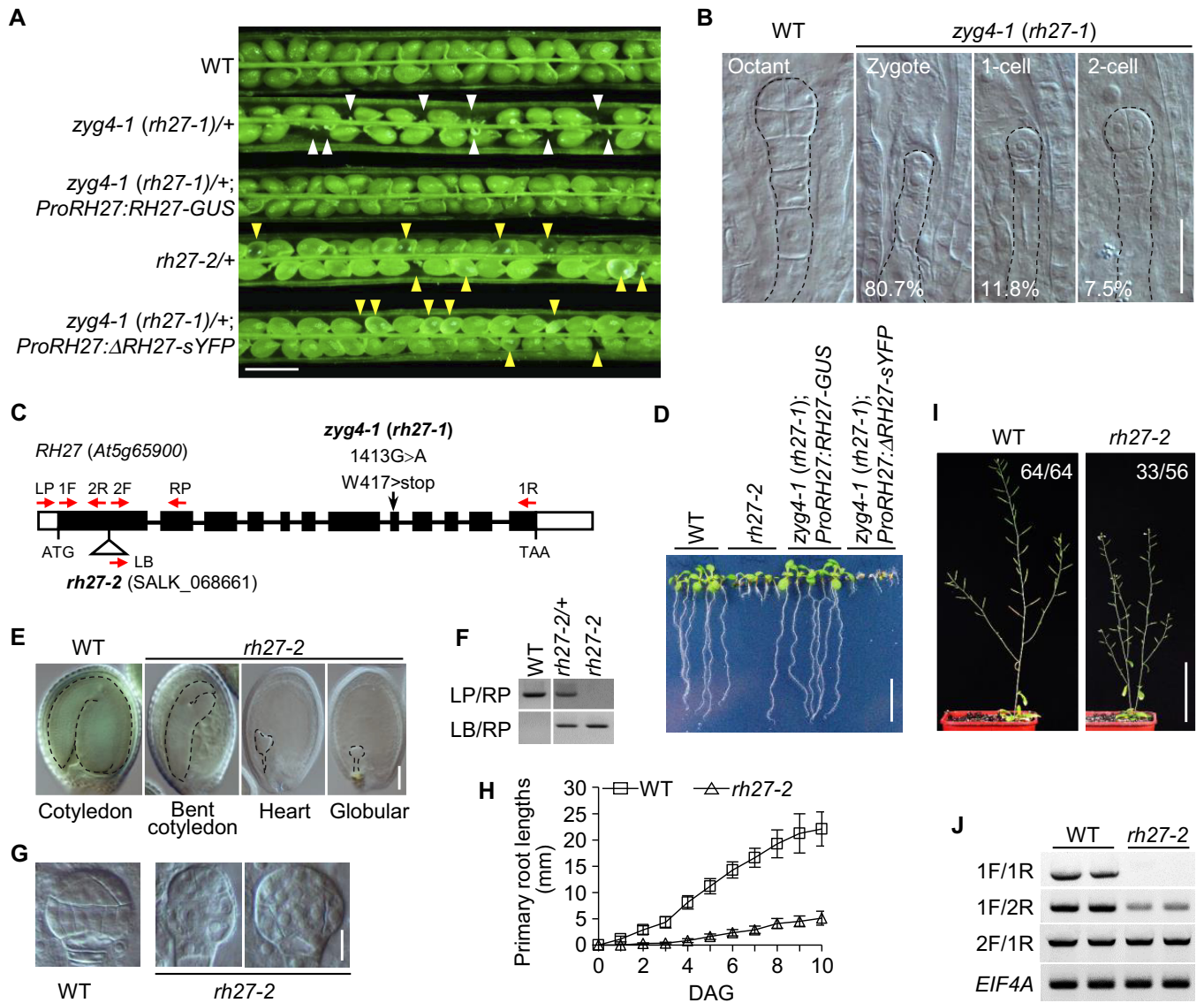


Figure 1 Phenotypes of the *zyg4* (*rh27*) Mutants. (A) Siliques of the following lines: wild-type (WT), *zyg4-1* (*rh27-1*)/+ with early aborted ovules (white arrowheads), *zyg4-1* (*rh27-1*)/+ carrying *ProRH27:RH27-GUS*, *rh27-2*/+ with late aborted ovules (yellow arrowheads), and *zyg4-1* (*rh27-1*)/+ carrying *ProRH27:ΔRH27-sYFP* lines. Note the full complementation of the *zyg4-1* (*rh27-1*) phenotype by *ProRH27:RH27-GUS*, while late aborted ovules (yellow arrowheads) were still observed in the siliques of *zyg4-1* (*rh27-1*)/+ plants carrying *ProRH27:ΔRH27-sYFP*. $\Delta RH27$ has a 310-bp deletion from the start codon of *RH27*, as found in *rh27-2*. Bar = 1 mm. (B) Nomarski images of whole-mount cleared ovules carrying wild-type and *zyg4-1* (*rh27-1*) embryos at 2 DAP. Unlike the wild-type siblings at the octant stage, the *zyg4-1* (*rh27-1*) embryos were arrested at the zygote, 1-cell, or 2-cell stage. The percentages of embryos arrested at different stages in aborted ovules are shown. Bar = 25 μ m. (C) Schematic illustration of the *RH27* gene. The open and black boxes indicate the untranslated and coding regions, respectively. The horizontal lines indicate introns. The G-to-A mutation in *zyg4-1* (*rh27-1*) and the T-DNA insertion in *rh27-2* are shown. The red arrows indicate positions of the primers used in (F) and (J). (D) Seedlings of the wild-type, *rh27-2*, *zyg4-1* (*rh27-1*); *ProRH27:RH27-GUS*, and *zyg4-1* (*rh27-1*); *ProRH27:ΔRH27-sYFP* lines at 6 DAG. Note that full complementation of *zyg4-1* was achieved using *ProRH27:RH27-GUS*, but only a partial complementation (with a phenotype similar to that of *rh27-2*) was observed when *ProRH27:ΔRH27-sYFP* was used. Bar = 1 cm. (E) Nomarski images of whole-mount cleared ovules carrying wild-type or *rh27-2* embryos at 14 DAP. Bar = 100 μ m. (F) PCR-based genotyping of *rh27-2* to show the successful insertion between the LP and RP primers. (G) Nomarski images showing abnormal cell division patterns in the *rh27-2* line at 3 DAP, compared with their wild-type siblings in the same silique. Bar = 10 μ m. (H) Primary root lengths of wild-type and *rh27-2* plants in the first 10 DAG. For each genotype, data are shown as the mean \pm SD of the primary root length (from at least 40 different roots). (I) Wild-type and *rh27-2* plants at 40 DAG, showing that two shoots formed simultaneously in the *rh27-2* plant. The numbers denote the frequencies of the phenotype shown. Bar = 10 cm. (J) RT-PCR analyses of *RH27* transcripts in the *rh27-2* line. Note that the full-length *RH27* transcript was not detectable in *rh27-2*, but the transcripts upstream and downstream of the T-DNA insertion were detected. *EIF4A* was used as an internal control. The primers used are indicated in (C).

Table 1 Genetic analyses of *zyg4* (*rh27*) mutants

Cross combinations		Aborted ovules (%)*	Total ovules examined	P value**
Female	Male			
<i>zyg4-1</i> (<i>rh27-1</i>)/+	<i>zyg4-1</i> (<i>rh27-1</i>)/+	26.1	621	0.53
<i>rh27-2</i> /+	<i>rh27-2</i> /+	24.4	1625	0.60
<i>zyg4-1</i> (<i>rh27-1</i>)/+	<i>rh27-2</i> /+	25.9	984	0.51
<i>rh27-2</i> /+	<i>zyg4-1</i> (<i>rh27-1</i>)/+	23.4	1068	0.23
wild-type (Col-0)	wild-type (Col-0)	2.9	137	n.a.

*The percentages of total ovules that were aborted or developmentally delayed, as counted under a dissection microscope.

**P-values were calculated from χ^2 tests for the 3:1 segregation.

n.a.: not applicable.

sequence and Δ RH27 that was in-frame fused to the N-terminus of *super Yellow Fluorescence Protein* (sYFP; *ProRH27:ΔRH27-sYFP*) was generated and introduced to wild-type Arabidopsis through floral dip (Clough and Bent, 1998). A transgenic line with a homozygous single insertion was identified and crossed with the *rh27-1*/+ line. In siliques of *rh27-1*/+ plants carrying homozygous *ProRH27:ΔRH27-sYFP*, a late embryo-defective phenotype resembling that of the *rh27-2*/+ line was observed (Figure 1, A). In addition, homozygous *rh27-1* seedlings carrying *ProRH27:ΔRH27-sYFP* (Supplemental Figure S2) were recovered and showed a *rh27-2*-like phenotype (Figure 1, D). Together, these data confirmed that Δ RH27 is a partially functional protein.

To elucidate the role of RH27 in post-embryonic growth and development, we performed detailed phenotypic analyses of *rh27-2* seedlings. Whole-mount clearing of root tips at 5 days after germination (DAG) revealed that the length of the root meristematic zone in *rh27-2* seedlings was much shorter than that in wild-type seedlings (Figure 2, A and B), and the meristem cell number, defined by the number of non-vacuolated cells in the cortex cell lineage (Casamitjana-Martínez et al., 2003), was also significantly lower in the mutant seedlings (Figure 2, C). By confocal examination of propidium iodide-stained roots, we observed an irregular organization of cell patterning in the meristematic zone of *rh27-2* roots (Figure 2, D), as well as frequent cell death, indicated by intensive propidium iodide penetration (Truernit and Haseloff, 2008), in cells adjacent to and above the QC (Figure 2, D and E, indicated by open arrowheads).

To analyze the cellular organization in *rh27-2* roots further, we introduced the *ProWOX5:erGFP* marker, in which an endoplasmic reticulum-localized green fluorescent protein (erGFP) was expressed under the control of the WOX5 promoter (Sarkar et al., 2007), to the *rh27-2* line by crossing. When examined under a confocal microscope at 1, 3, 5, and 7 DAG, instead of the well-defined *ProWOX5:erGFP*-positive QC cells observed in the wild-type roots, the pattern of *ProWOX5:erGFP*-positive cells in *rh27-2* roots was altered greatly, with erGFP-positive cells located not only in QC cells, but also in those above the QC (Figure 2, E; Supplemental Figure S4). Next, we counted the number of erGFP-positive cells in serial confocal sections. In wild-type roots, an average of four erGFP-positive cells was observed consistently (Figure 2, F), while

in *rh27-2* roots, 6.6 ± 1.5 ($n = 5$), 11 ± 2.3 ($n = 7$), 9.7 ± 2.4 ($n = 7$), and 8.6 ± 3.0 ($n = 8$) erGFP-positive cells were observed at 1, 3, 5, and 7 DAG, respectively (Figure 2, F). We then used Lugol staining to examine the columella stem cells (CSCs) located underneath the QC, and observed that starch granules were accumulated in expected CSC regions in 85.4% of *rh27-2* roots ($n = 41$; Figure 2, G), suggesting premature differentiation of the CSCs. By contrast, this phenomenon was not observed in wild-type roots ($n = 29$; Figure 2, G). These results suggest that stem cell homeostasis was disrupted in the RAM of the *rh27-2* line.

Next, we performed whole-mount clearing of shoot apices and observed that the SAMs in *rh27-2* plants were small, flat, and occasionally displayed twin domes, unlike the single dome structures in the wild-type shoots (Supplemental Figure S5, A). Subsequently, we introduced *ProCLV3:GUS*, a marker for stem cells (Fletcher et al., 1999), and *ProWUS:GUS*, a marker for the SCOC (Mayer et al., 1998), to the *rh27-2* line by crossing. A GUS assay revealed highly irregular GUS staining patterns in the SAMs of *rh27-2* seedlings carrying *ProCLV3:GUS*, whereas wild-type seedlings displayed a well-defined stem cell domain (Supplemental Figure S5, B). Median sectioning across the SAM revealed that, compared with the wild-type plants, the *rh27-2* plants carrying *ProCLV3:GUS* displayed a reduced number of *ProCLV3:GUS*-positive stem cells that were scattered in SAMs (Figure 3, A). Statistical analyses showed that, when examined at 1, 3, 5, and 7 DAG, the SAMs in *rh27-2* plants had significantly fewer L1 cells with GUS signals than those in wild-type plants (Figure 3, B). However, ImageJ analyses (Schindelin et al., 2012) revealed that the GUS-positive cells in the L1 layer of *rh27-2* plants were significantly larger than those in the wild-type plants (Figure 3, C). Similarly, GUS assays performed in wild-type and *rh27-2* plants carrying *ProWUS:GUS* showed that, when examined at 3, 5, and 7 DAG, the intensity and pattern of the GUS signal varied greatly in the *rh27-2* line (Figure 3, D and Supplemental Figure S6, A and B). A GUS signal was occasionally observed in the L1 layer of the SAMs in *rh27-2* plants (Supplemental Figure S6, B, indicated by arrowheads), but was not observed in the corresponding region of wild-type plants. Taken together, these results suggest that stem cell homeostasis was disrupted in the RAM and SAM of *rh27-2* plants.

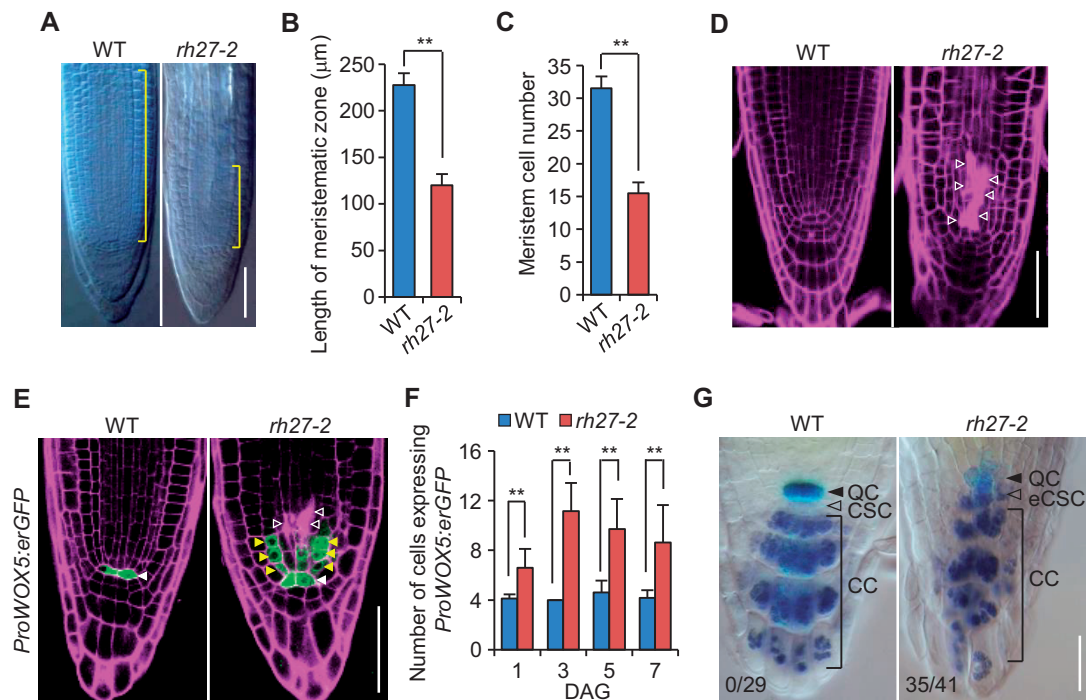


Figure 2 Abnormal root development and defective stem cell homeostasis in the *rh27-2* line. (A) Nomarski images of root tips from wild-type (WT) and *rh27-2* plants at 5 DAG. Brackets indicate the meristematic zone. Bar = 50 μm. (B) and (C) The average lengths of the meristematic zones (B, $n = 20$) and the average numbers of meristematic cells (C, defined by the number of non-vacuolated cells in the cortex cell lineage, $n = 40$) in wild-type and *rh27-2* roots at 5 DAG. Error bars indicate the SD and asterisks indicate significant differences between samples (two-tailed Student's *t* test, $**P < 0.01$). (D) and (E) The cellular organization (D) and expression of *ProWOX5:erGFP* (green; E) in wild-type and *rh27-2* root meristems at 5 DAG, examined under a confocal microscope. Propidium iodide (magenta) staining was used to show the cellular structure. Note the increased number of GFP-positive cells (yellow arrowheads), located above the QC (white arrowheads), in *rh27-2* root meristems (E). Dead cells were observed frequently in *rh27-2* root meristems (open arrowheads). Bar = 50 μm. (F) The numbers of cells expressing *ProWOX5:erGFP* in wild-type and *rh27-2* root meristems. Data are shown as the mean \pm SD of the number of *ProWOX5:erGFP*-positive cells in at least five roots. Asterisks indicate significant differences between the samples (two-tailed Student's *t* test, $**P < 0.01$). (G) Examinations of *QC25:GUS* expression (blue) and starch grain accumulation (brownish blue) in wild-type and *rh27-2* roots at 5 DAG. Starch grain accumulation was observed frequently in the expected CSC (eCSC) of *rh27-2* roots but was not observed in CSC of the wild-type roots. The numbers denote the frequencies of CSC or eCSC with starch grains. CC, columella cell. Bar = 50 μm.

RH27 is expressed in embryos from the zygote stage onwards, and in the SAM and RAM

The introduction of a *ProRH27:RH27-sYFP* construct was able to complement the short-root phenotype of the *rh27-2* mutant (Supplemental Figure S7, A). Immunoblot analyses using an anti-RH27 antibody showed that the full-length RH27-sYFP fusion protein was expressed in *rh27-2*; *ProRH27:RH27-sYFP* transgenic plants (Supplemental Figure S7, B), suggesting that the regulatory sequence used in *ProRH27:RH27-sYFP* carries all essential elements and that the RH27-sYFP fusion protein is functional. Confocal examination of *ProRH27:RH27-sYFP* transgenic plants showed that, during the reproductive stage, RH27-sYFP was expressed in mature ovules (Supplemental Figure S7, C), as well as unicellular and bicellular microspores, but was absent from mature pollen (Supplemental Figure S7, D).

During embryogenesis, RH27-sYFP expression was detected in the nuclei of the zygote staged embryos (Figure 4, A), and then in embryos at the 2-cell, 4-cell, globular, and torpedo-shaped stages (Figure 4, B–E). Examination of ovules excised from transgenic plants carrying the egg cell-specific marker

pEC1:H2B-RFP (Ingouff et al., 2009) and pollinated by pollens from *ProRH27:RH27-sYFP* plants showed that expression of the paternal RH27-sYFP was activated at the zygote stage (Supplemental Figure S7, E).

Next, the expression of RH27 during post-embryonic development was examined using *ProRH27:RH27-GUS* transgenic plants. RH27-GUS was actively expressed in shoot apices and root tips (Supplemental Figure S8, A). In the inflorescence, RH27-GUS signals were detected in floral primordia, young flowers, and pistils (Supplemental Figure S8, B). Semi-thin sectioning of shoot apices of *ProRH27:RH27-GUS* plants after GUS assays revealed that RH27-GUS was expressed in SAMs and young leaves (Figure 4, F). Confocal examination of roots from *ProRH27:RH27-sYFP* seedlings showed that RH27-sYFP signals were primarily located in the nuclei of RAM cells but were excluded from QC cells (Figure 4, G). Further examination of root epidermal cells in *ProRH27:RH27-sYFP* seedlings, counterstained with Hoechst 33258, showed that the RH27-sYFP protein was localized primarily in the nucleolus (Figure 4, H).

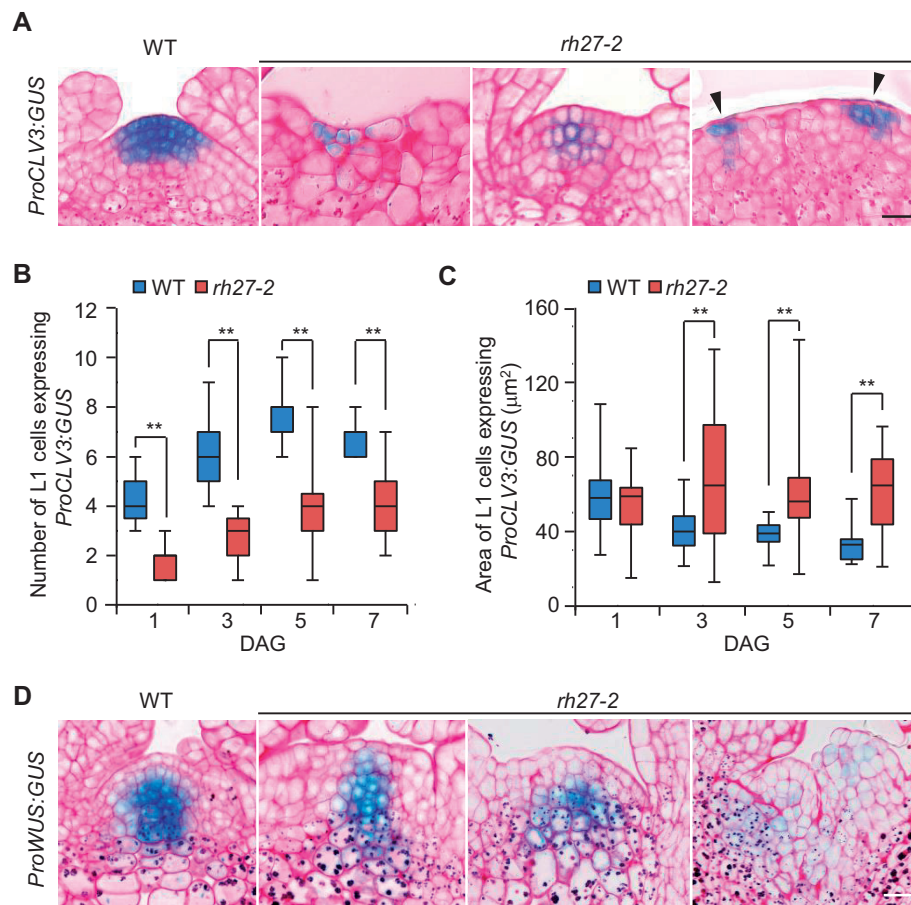


Figure 3 Stem cell homeostasis is defective in the SAM of *rh27-2* plants. (A) Median sections of SAMs of wild-type (WT) and *rh27-2* seedlings carrying *ProCLV3:GUS*, showing the presence of stem cells. Arrowheads indicate two GUS-positive domains in a SAM of a *rh27-2* seedling. Sections from 24 shoot apices were examined for *rh27-2*. Bar = 20 µm. (B) and (C) Box plot diagrams showing the numbers (B) and areas (C) of GUS-positive L1 cells in median sections of SAMs from wild-type and *rh27-2* plants carrying *ProCLV3:GUS*. Data are shown as the mean ± SD of the numbers of cells in at least 12 SAMs from each stage (B), and the areas of GUS-positive cells from at least 3 SAMs (C). Asterisks indicate significant differences between samples (two-tailed Student's *t* test, ***P* < 0.01). (D) Median sections of wild-type and *rh27-2* SAMs from 7 DAG seedlings carrying *ProWUS:GUS*, showing the SCOC in the SAM. Note the diffuse expression pattern of *ProWUS:GUS* in the *rh27-2* SAMs. Sections from 12 shoot apices were observed for *rh27-2*. Bar = 20 µm. In (A) and (D), sections were stained with periodic acid-Schiff (pink) to show the cellular structure.

The *rh27-2* mutant displays reduced levels of miRNAs and increased levels of their target genes in shoot apices and root tips

Since DEAD-box RNA helicases play an important role in miRNA biogenesis in animals (Han et al., 2014; Yin et al., 2015; Zhao et al., 2016), we used RT-quantitative PCR (RT-qPCR) analyses (Shi and Chiang, 2005) to examine the accumulations of miRNAs in *rh27-2* plants. The abundances of the SAM-related miRNAs miR171 and miR164 in *rh27-2* shoot apices were lower than those in wild-type shoot apices (Figure 5, A). Similarly, the abundances of the RAM-related miRNAs miR165 and miR166 in *rh27-2* root tips were lower than those in wild-type root tips (Figure 5, A). Next, in situ hybridization was performed to examine the accumulation patterns of miRNAs in shoot apices using digoxigenin-labeled LNA oligo probes. In wild-type shoots, an antisense probe detected miR164 in cytoplasm-dense cells of the leaf

primordia (Figure 5, B, left). By contrast, in *rh27-2* shoots, miR164 was present in a dispersed pattern in vacuolated cells of the shoot apices (Figure 5, B, right).

To determine whether the altered abundances of miRNAs in the *rh27-2* line affect the expression of their target genes, RT-qPCR analyses were performed to examine the transcript levels of *HAM1* and *CUCs* (*CUC1*, *CUC2*, and *NAC100*), which are targets of miR171 and miR164, respectively (Llave et al., 2002; Mallory et al., 2004a), in shoot apices from wild-type and *rh27-2* seedlings at 5 DAG. In addition, the transcript levels of the *HD-ZIP III* family members *PHB*, *PHV*, *CNA*, and *REV*, which are targets of miR165/166 (Mallory et al., 2004b), were examined in root tips from both lines. Compared with those in shoot apices from wild-type plants, the levels of *HAM1*, *CUC1*, *CUC2*, and *NAC100* were up-regulated in shoot apices from *rh27-2* plants, and that of *PHB* was higher in root tips from *rh27-2* plants than those from wild-type

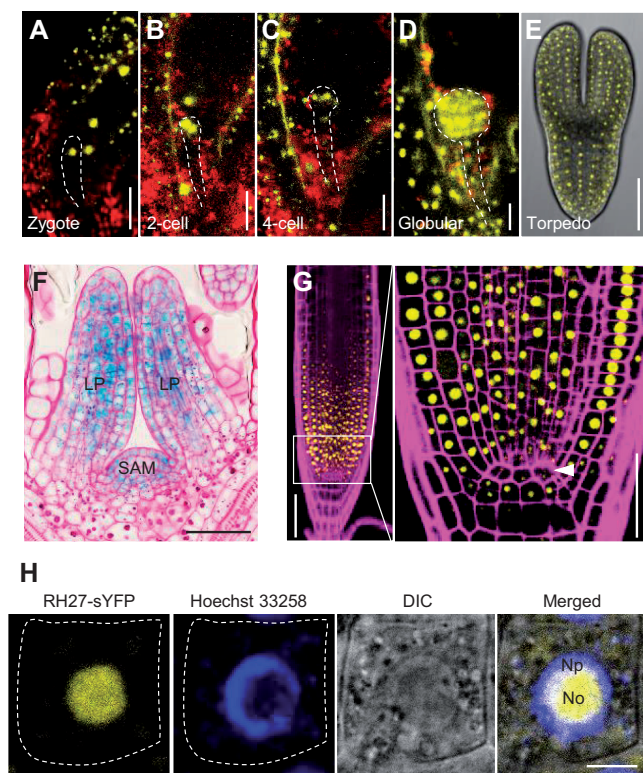


Figure 4 Expression and subcellular localization of RH27 in Arabidopsis. (A–E) Expression of *ProRH27:RH27-sYFP* (yellow) in embryos at the zygote (A), 2-cell (B), 4-cell (C), globular (D), and torpedo-shaped (E) stages. Note the nuclear localization of the RH27-sYFP signals. Red, auto-fluorescence. Dashed lines outline the embryos. Bars = 20 μm for (A) to (D), and 50 μm for (E). (F) Expression of *ProRH27:RH27-GUS* (blue) in the shoot apex, specifically the SAM and leaf primordia (LP). The section was stained with periodic acid-Schiff (pink) to show the cellular structure. Bar = 50 μm . (G) Expression of *ProRH27:RH27-sYFP* (yellow) in the RAM. Part of the meristematic zone (framed) is magnified (right) to show the presence of RH27-sYFP in meristematic cells, but not the QC (arrowhead). The root was stained with propidium iodide (magenta) to show the cellular structure. Bars = 50 μm . (H) Subcellular localization of the RH27-sYFP protein (yellow) in a root epidermal cell from a transgenic plant carrying *ProRH27:RH27-sYFP*. The nucleus was stained with Hoechst 33258 (blue). Note that RH27-sYFP was localized primarily in the nucleolus (No) and to a small degree in the nucleoplasmic region (Np). Dotted lines outline the cell boundary. Bar = 5 μm .

plants (Figure 5, C). In situ hybridization analyses of shoot apices using sense and antisense probes showed that *CUC2* transcript was present at the boundaries between the SAM and leaf primordia (Figure 5, D, indicated by arrowheads), as reported previously (Ishida et al., 2000). However, in *rh27-2* shoot apices, a diffused pattern and no evident boundary-specific expression were observed (Figure 5, D; Supplemental Figure S9).

To investigate the effect of the *rh27-2* mutation on miRNA biogenesis in general, small RNA-seq was performed to analyze the levels of miRNAs in shoot apices and root tips excised from the wild-type and *rh27-2* seedlings at 5 DAG. Data from three independent experiments for each

set of samples were reproducible (Supplemental Figure S10). Among the 428 known miRNAs in Arabidopsis (<http://www.mirbase.org/>), 207 were detected in shoot apices and 81 were down-regulated in the *rh27-2* line (Figure 5, E and Supplemental Data Set S1), including miR171 and miR394, which have well-known roles in stem cell homeostasis in the SAM (Knauer et al., 2013; Zhou et al., 2018). In root tips, 269 miRNAs were detected, of which 154 were down-regulated in the *rh27-2* line (Figure 5, F and Supplemental Data Set S1). Notably, smaller numbers of miRNAs were up-regulated in the *rh27-2* line: 60 and 63 in shoot apices and root tips, respectively. Furthermore, RNA-seq analyses of wild-type and *rh27-2* seedlings at 5 DAG showed that 18 miRNA target genes were up-regulated in shoot apices and 31 were up-regulated in root tips of *rh27-2* seedlings (Supplemental Figure S11, A and B).

RH27 is involved in pri-miRNA processing

To explore the function of RH27 in miRNA biogenesis further, RT-qPCR analyses were performed to examine the levels of several pri-miRNAs in shoot apices and root tips of wild-type and *rh27-2* seedlings at 5 DAG. All seven pri-miRNAs examined in the shoot apices were accumulated at lower levels in the *rh27-2* than in the wild-type line (Figure 6, A). Similarly, five of the seven pri-miRNAs examined in root tips showed reduced levels of transcript in *rh27-2* seedlings (Figure 6, A and Supplemental Figure S12, A). An RNA-seq analysis revealed that, among the 116 and 65 pri-miRNAs detected in shoot apices and root tips, 29 and 7 were down-regulated, respectively, in *rh27-2* seedlings (Supplemental Figure S12, B and C).

We then examined whether RH27 is associated with pri-miRNAs in vivo using RNA immunoprecipitation-coupled RT-PCR (RIP-RT-PCR). All four pri-miRNAs examined (pri-miR164a, pri-miR165a, pri-miR166a, and pri-miR171b) were co-precipitated by the anti-RH27 antibody (Figure 6, B), whereas no or very weak signals were obtained when no antibody was applied as a control. In addition, no precipitation signal was observed when *UBIQUITIN 5* (*UBQ5*) primers were used as a negative control (Figure 6, B). Overall, these data suggest that RH27 is involved in pri-miRNA processing.

RH27 interacts with DDL, HYL1, and SE

In animals, DEAD-box RNA helicases act as components of the microprocessor complex to regulate miRNA biogenesis (Gregory et al., 2004). In plants, the microprocessor complex consists of DCL1, SE, and HYL1. In addition, DDL interacts with DCL1 to facilitate the recruitment of substrates of the microprocessor complex (Yu et al., 2008). To determine whether RH27 interacts with these components, in vitro pull-down assays were performed using glutathione S-transferase (GST)-tagged DCL1, DDL, HYL1, or SE as the bait, and His-tagged RH27 as the prey. GST-DCL1, GST-DDL, GST-HYL, and GST-SE were able to pull-down RH27-His, whereas GST alone was not (Figure 7, A). Subsequently, a co-immunoprecipitation experiment was performed to examine the interactions of RH27 with DCL1, DDL, HYL1, and SE

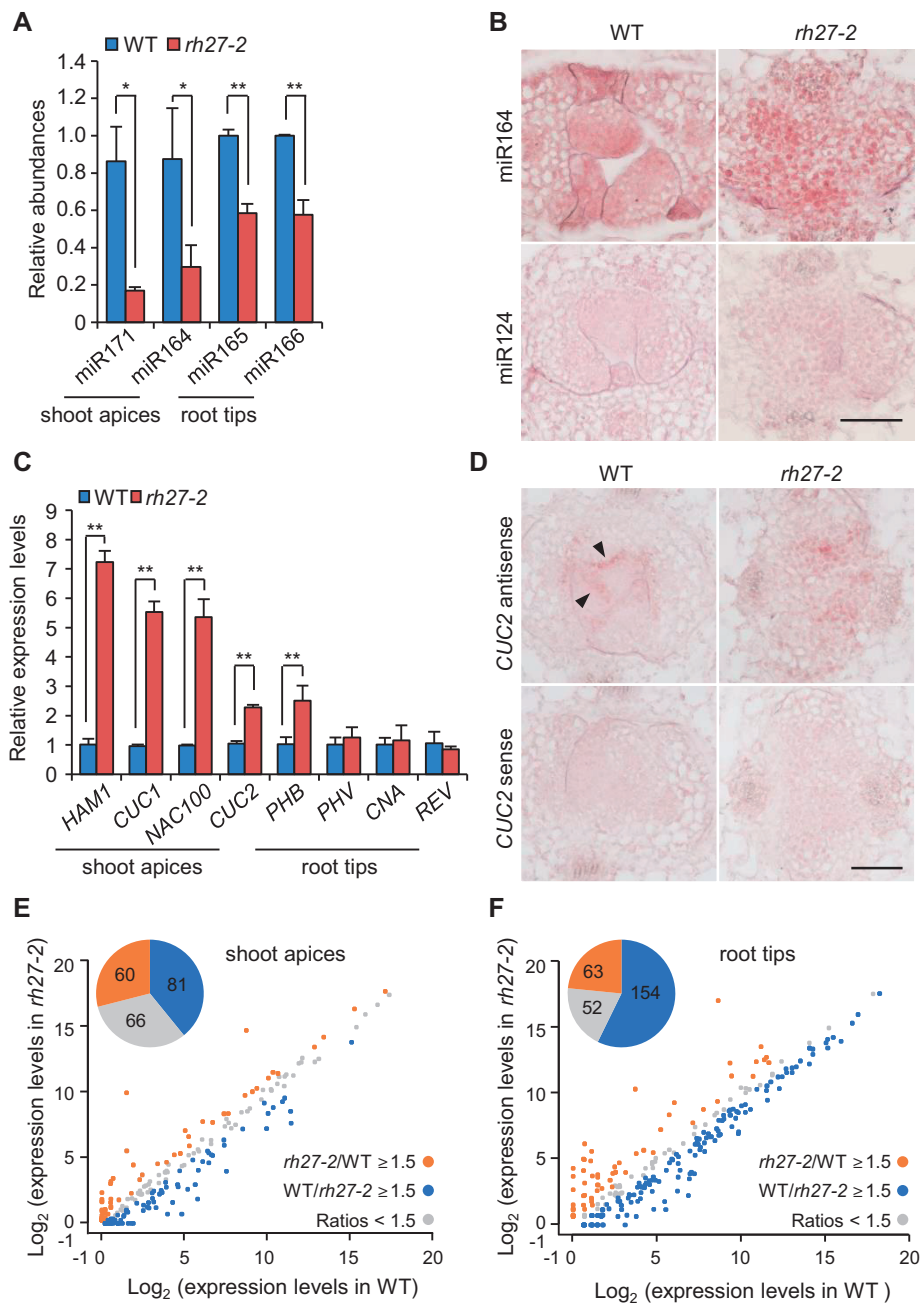


Figure 5 Accumulation and expression patterns of miRNAs and their target genes in *rh27-2* seedlings. (A) Quantification of miRNAs in shoot apices and root tips of wild-type (WT) and *rh27-2* seedlings by RT-qPCR. The expression levels were normalized to those of 5.8S rRNA (shoot apices) or U6 (root tips). (B) In situ hybridization analyses of miR164 in shoot apices from wild-type and *rh27-2* plants at 5 DAG. Note the diffused expression of miR164 in vacuolated cells of *rh27-2* shoots, compared with the specific expression pattern in cytoplasm-dense cells in the leaf primordia of wild-type shoots. A miR124 antisense probe from mouse was used as a negative control. Bar = 50 μ m. (C) RT-qPCR analyses of the transcript levels of genes involved in stem cell homeostasis in the SAM and RAM. Note that the expression levels of *HAM1* (a target of miR171), *CUC1*, *CUC2*, and *NAC100* (targets of miR164), and *PHB* (a target of miR165/166) were up-regulated in *rh27-2* plants. The expression levels were normalized to that of *EIF4A*. (D) In situ hybridization analyses using an antisense probe, showing the expression patterns of *CUC2* in shoot apices from wild-type and *rh27-2* seedlings. Note the diffused expression of *CUC2* in *rh27-2* shoots, compared with the boundary-specific expression (arrowheads) between the SAM and leaf primordia in wild-type shoots. A *CUC2* sense probe was used as a negative control. Bar = 50 μ m. (E) and (F) Comparison of the levels of miRNAs in wild-type and *rh27-2* shoot apices (E) and root tips (F), as determined by small RNA-seq. Note that, compared with the wild-type shoot apices, 81 (blue) and 60 (orange) miRNAs were down-regulated and up-regulated (≥ 1.5 -fold) in *rh27-2* shoot apices, respectively (E). In addition, 154 (blue) and 63 (orange) miRNAs were down-regulated and up-regulated (≥ 1.5 -fold) in *rh27-2* root tips, respectively (F). In (A) and (C), the error bars indicate the SD from three independent samples. In each experiment, three independent repeats were conducted for each sample. Asterisks indicate significant differences between samples (two-tailed Student's *t* test, **P* < 0.05, ***P* < 0.01).

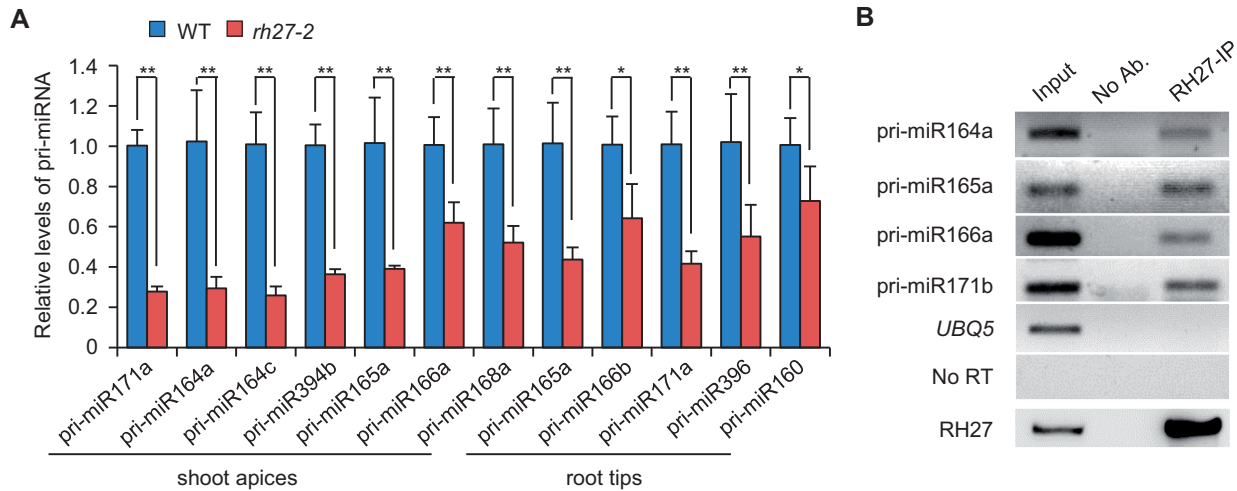


Figure 6 Involvement of RH27 in pri-miRNA processing. (A) RT-qPCR analyses of pri-miRNAs in shoot apices and root tips of wild-type (WT) and *rh27-2* seedlings. Error bars indicate the SD of three independent samples. Asterisks indicate significant differences from the wild-type (two-tailed Student's *t* test, * $P < 0.05$, ** $P < 0.01$). (B) A RIP-RT-PCR assay using an anti-RH27 antibody to show the association of RH27 with pri-miR164a, pri-miR165a, pri-miR166a, and pri-miR171b in vivo. One-tenth of the RNA, as used in the RIP-RT-PCR analysis, was used as the input sample. No Ab.: No antibody control. In the bottom panel, the anti-RH27 antibody was used to show the presence of RH27 proteins in the input and RH27-IP samples. No RT: RIP-RT-PCR was performed with pri-miR166a primers without reverse transcription. UBQ5, negative control.

in vivo. In transient assays performed pair-wisely in *Nicotiana benthamiana* leaves, RH27-Flag was detected in precipitates of DCL1-Myc, DDL-Myc, HYL1-Myc, and SE-Myc. No interaction was detected when either the empty Myc vector or NAC81-Myc was used (Figure 7, B).

To validate the interactions in vivo, pair-wise firefly luciferase complementation imaging (LCI) assays (Chen et al., 2008) were performed in *N. benthamiana* using RH27-nLUC with one of the cLUC constructs (cLUC-DCL, cLUC-DDL, cLUC-HYL1, or cLUC-SE) or cLUC-AGO1 as a control. Strong interactions were observed for the combinations of RH27-nLUC and cLUC-DDL, RH27-nLUC and cLUC-HYL1, and RH27-nLUC and cLUC-SE (Figure 7, C). A weak interaction was also detected when RH27-nLUC and cLUC-DCL1 were co-infiltrated (Figure 7, C), while no interaction was detected when RH27-nLUC and cLUC-AGO1 were co-infiltrated (Figure 7, C). We then examined the interaction between RH27 and DCL1, DDL, HYL1, or SE using bimolecular fluorescence complementation (BiFC) assays (Walter et al., 2004). RH27 was able to interact with DDL, HYL1, and SE, but no interaction between RH27 and DCL1 was detected (Figure 7, D). It should be noted that the interaction signals were localized exclusively in discrete bodies, most likely nuclear dicing bodies (Fang and Spector, 2007; Song et al., 2007; Figure 7, D).

A further genetic analysis was performed by introducing the *rh27-2* mutation into the *se-1* or *hyl1-2* mutant line by crossing. Phenotypic analysis of homozygous *rh27-2 se-1* and *rh27-2 hyl1-2* double mutants identified in the F2 progenies showed that the defects in growth and development were more severe in both double mutants than in any of the single mutants (Figure 7, E), suggesting an additive role of RH27, SE, and HYL1 in miRNA biogenesis.

Discussion

Studies performed over the past two decades have identified more than 10 genes that are essential for zygote division and are involved in cell cycle regulation, energy supply, and ribosomal RNA and tRNA processing (Shen et al., 2002; Xu et al., 2005; Lin et al., 2007; Ronceret et al., 2008; Andreuzza et al., 2010; Li et al., 2010; Ngo et al., 2012; Wu et al., 2012; Yu et al., 2012; Guo et al., 2016; Yang et al., 2017). In this study, we established that the *zyg4-1* (*rh27-1*) mutant of Arabidopsis exhibits a zygote-lethal phenotype caused by a point mutation in the DEAD-box RNA helicase-coding gene RH27. Although this gene is not expressed in sperm cells of mature pollen, both the paternal and the maternal RH27 alleles are expressed immediately after fertilization. The contributions of maternal and paternal genomes to early zygotic embryogenesis have been disputed (Autran et al., 2011; Nodine and Bartel, 2012; Del Toro-De León et al., 2014; Zhao et al., 2019); however, the observed maternal and paternal RH27 expression in zygotes and the typical Mendelian inheritance of the *zyg4-1* (*rh27-1*) mutation support the model of equal contributions of the two parental genomes.

As a family of highly conserved enzymes present in almost all living organisms, DEAD-box RNA helicases are involved in a range of processes, such as tumorigenesis, germ cell specification, and embryonic patterning, through the regulation of RNA metabolism (Schübach and Wieschaus, 1986; Botlagunta et al., 2008; Linder and Jankowsky, 2011; Cai et al., 2017). In plants, DEAD-box RNA helicases are implicated in drought tolerance, salinity sensitivity, and cold and heat responses (Gong et al., 2005; Khan et al., 2014; Zhu et al., 2015; Wang et al., 2016, 2019a). In this study, we observed that the weak allele of *rh27-2*, containing a T-DNA

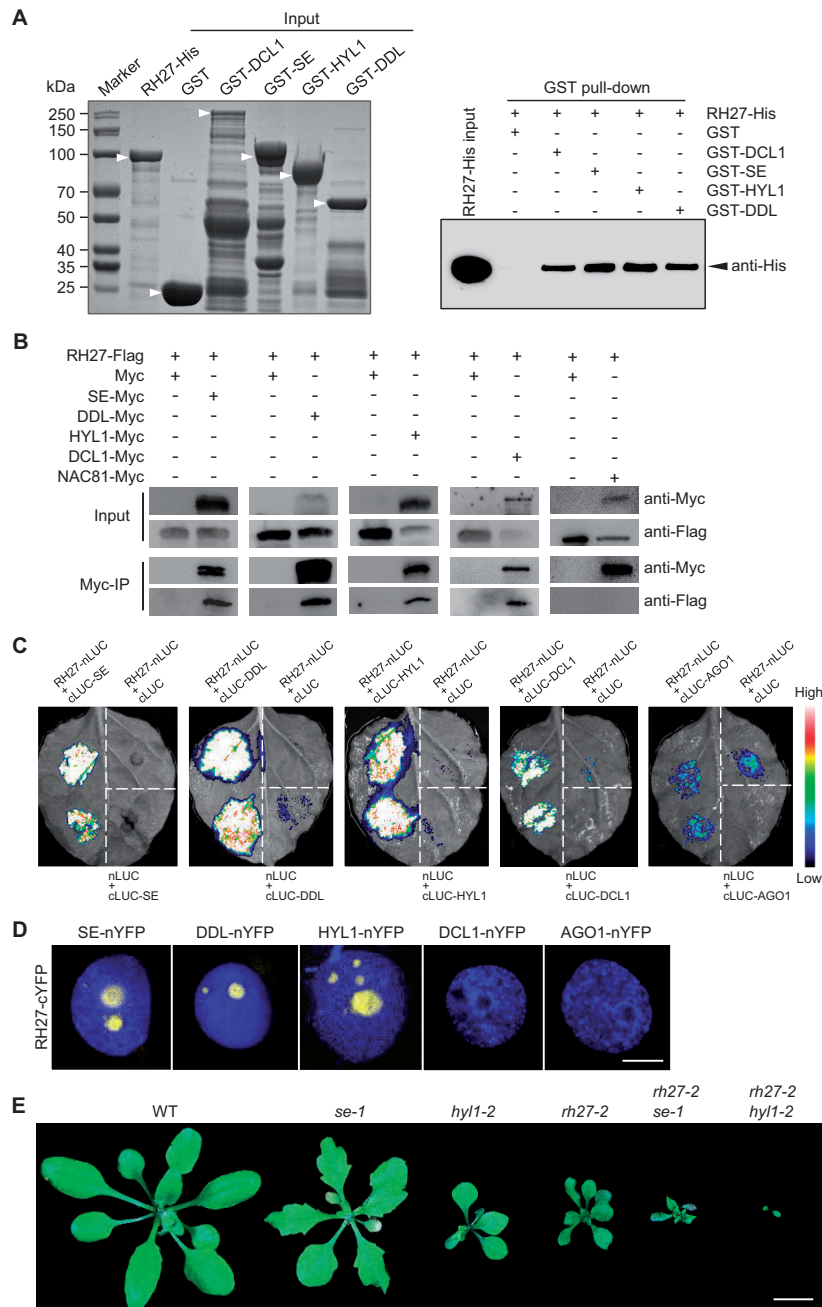


Figure 7 RH27 interacts with DDL, HYL1, and SE. (A) In vitro pull-down assays using His-tagged RH27 (RH27-His) as prey, and GST-tagged DCL1, DDL, HYL1, or SE as bait, to examine the interaction of RH27 with miRNA biogenesis components. GST alone was used as a negative control. The left panel, a PAGE gel stained with Coomassie Bright Blue, shows heterologous production of input proteins with expected molecular weights (arrowheads) produced in *Escherichia coli*. The right panel shows that the RH27-His protein (arrowhead) was pulled-down by GST-DCL1, GST-DDL, GST-HYL1, and GST-SE, using glutathione MagBeads, as detected by the anti-His antibody. Three independent experiments were performed. (B) Co-immunoprecipitation experiments to examine the interaction of Flag-tagged RH27 with Myc-tagged DCL1, DDL, HYL1, or SE. The assays were performed by pair-wise co-infiltration of constructs in *N. benthamiana* leaves. Note that RH27-Flag was precipitated by DCL1-Myc, DDL-Myc, HYL1-Myc, and SE-Myc, but not by the controls: empty Myc vector (Myc) and NAC81 transcription factor fused with Myc (NAC81-Myc). Three independent experiments were performed. (C) LCI assays performed in *N. benthamiana* leaves to examine the interaction of RH27 with DCL1, DDL, HYL1, or SE. The indicated constructs were co-infiltrated. AGO1 was used as a negative control. Note the strong interactions between RH27-nLUC and cLUC-DDL, RH27-nLUC and cLUC-HYL1, and RH27-nLUC and cLUC-SE. A weak interaction was observed between RH27-nLUC and cLUC-DCL1. Three independent experiments were performed for each combination, and in each experiment, more than three leaves were infiltrated and examined. (D) A BiFC assay performed in *N. benthamiana* leaves, examined under a confocal microscope, to detect the interaction between RH27-cYFP and DCL1-nYFP, DDL-nYFP, HYL1-nYFP, or SE-nYFP. AGO1-nYFP was used as a negative control. Note that BiFC signals (yellow) were detected in the nuclei in combinations of RH27-cYFP and DDL-nYFP, RH27-cYFP and HYL1-nYFP, and RH27-cYFP and SE-nYFP. No interaction was detected for RH27-cYFP and DCL1-cYFP. Nuclei were counterstained with 4',6-diamidino-2-phenylindole (DAPI; blue). Three independent experiments were performed. Bar = 5 μ m. (E) Phenotypes of the *se-1*, *hyl1-2*, and *rh27-2* single mutants, and the *rh27-2 se-1* and *rh27-2 hyl1-2* double mutants, at 25 DAG. Bar = 1 cm.

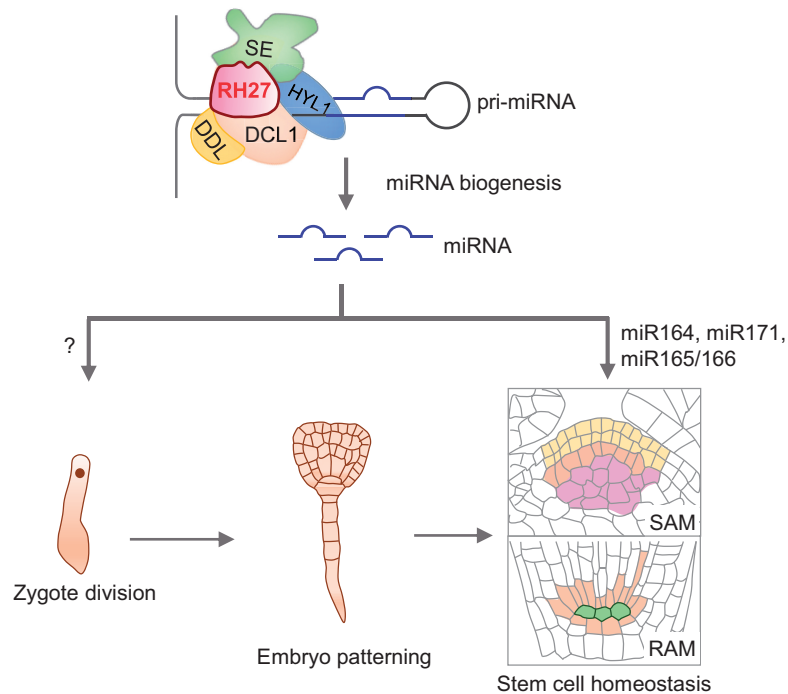


Figure 8 A proposed model for the role of RH27 in zygote division and stem cell homeostasis. Based on the facts that mutations of *RH27* caused a zygote-lethal phenotype (*rh27-1*) and defective stem cell homeostasis (*rh27-2*), and RH27 interacts with DDL, HYL1, and SE, associates with pri-miRNAs, and promotes the accumulations of miR164, miR171, and miR165/166, it is proposed that RH27 is a key player in zygote division, stem cell homeostasis and miRNA biogenesis in Arabidopsis. It should be noted that direct evidence for the involvement of miRNAs in zygote division is still lacking; therefore, a question mark is used.

insertion in *RH27* that causes truncation of the non-conserved N-terminal region of the RH27 protein, was defective in stem cell homeostasis in the SAM and RAM. Previous studies have demonstrated that stem cell-expressed CLV3 peptides, perceived by the CLV1/CLV2/RPK2 receptor kinases, establish a negative feedback regulation loop with the SCOC-expressed transcription factor *WUS* to maintain stem cell homeostasis in the SAM (Fletcher et al., 1999; Brand et al., 2000; Kinoshita et al., 2010). Here, homozygous *rh27-2* seedlings showed short-root and multi-shoot phenotypes, in which the dome structure of SAM was lost and the expression patterns of the stem cell marker gene *CLV3* and the SCOC marker gene *WUS* were irregular. Occasionally, multiple *CLV3* and *WUS* expression domains were identified in *rh27-2* plants, which is consistent with the formation of multiple shoots at the bolting stage. In the RAM, in contrast to the specific expression of *WOX5* in four QC cells observed in wild-type plants, disorganized *WOX5* expression, including increased *WOX5*-positive cell numbers and altered cell patterns, was observed in *rh27-2* plants. Similarly, altered *WOX5* expression has also been reported in plants expressing a mutant *ACTIVE QUIESCENT CENTER1* (*AQC1*) gene, which encodes a tyrosylprotein sulfotransferase involved in peptide modifications during root stem cell maintenance (Zhou et al., 2010). In addition, CSCs, the stem cells for the columella

cell lineage, were prematurely differentiated in *rh27-2* roots in this study. A similar phenotype has been observed following laser ablation of QC cells (van den Berg et al., 1997) or mutation of the *WOX5* or *AQC1* gene (Sarkar et al., 2007; Zhou et al., 2010). Overall, these results suggest that RH27 plays a critical role in stem cell homeostasis in both the SAM and RAM.

The *rh27-2* mutant had reduced levels of miR164 and miR171, and increased levels of the *CUC1*, *CUC2*, *NAC100*, and *HAM1* mRNAs in the shoot apices. *CUC1* and *CUC2*, targets of miR164, are redundantly required to define organ boundaries in the SAM (Takada et al., 2001; Rhoades et al., 2002; Mallory et al., 2004a). In this study, in situ hybridization analyses revealed that *CUC2* displayed a diffuse expression pattern in *rh27-2* plants, unlike the boundary-specific expression seen in wild-type plants. Similarly, miR164 also displayed a dispersed expression pattern in the *rh27-2* mutant, rather than the leaf primordium-specific expression seen in the wild-type line. It is possible that the altered expression pattern of *CUC2* is a consequence of changes in the expression level and pattern of miR164, and may lead to defective functioning of the SAM in *rh27-2* plants, as well as the multi-shoot phenotype. In addition, the up-regulation of *HAM1*, possibly caused by decreased expression of miR171, may also contribute to defective SAM function and stem cell

homeostasis in the *rh27-2* line. In agreement with this speculation, previous studies showed that mutations in miR164-coding genes, or expression of miR164-resistant *CUC2* (resulting in expanded expression region of *CUC2*), lead to altered phyllotaxis in the inflorescence and organ boundaries in flowers (Laufs et al., 2004; Sieber et al., 2007). In roots, *PHB* is a gene essential for xylem cell fate specification, and a gain-of-function mutant of *PHB* containing a point mutation at the miR165/166 target site shows a short-root phenotype (Carlsbecker et al., 2010). Consistent with the short-root phenotype in the gain-of-function mutant of *PHB*, we observed that *rh27-2* plants exhibited a similar short-root phenotype and an elevated expression level of *PHB*, alongside a reduced accumulation of miR165/166. It is reasonable to speculate that RH27-mediated miRNA biogenesis may control the expression of genes involved in stem cell homeostasis in the SAM and RAM (Figure 8).

In animals, DEAD-box RNA helicase is a component of the microprocessor complex (Gregory et al., 2004). In *Arabidopsis*, the microprocessor complex consisting of DCL1, HYL1, and SE (Wang et al., 2019b) recognizes and cleaves pri-miRNAs (Kurihara et al., 2006; Dong et al., 2008). The RNA-binding protein DDL is proposed to promote the access of DCL1 to its substrates (Yu et al., 2008). In this study, strong interactions of RH27 with DDL, HYL, and SE, and a weak interaction between RH27 and DCL1, were detected. It has been reported previously that DDL, HYL1, and SE bind to pri-miRNAs, and in this study, we established that RH27 binds to four different pri-miRNAs. These results led us to propose RH27 as a component of the microprocessor complex (Figure 8). Previous studies have shown that the *dcl1-1* and *se-4* mutant lines show embryo defects at the late globular stage (Schwartz et al., 1994; Lobbes et al., 2006), whereas the *zyg4-1* (*rh27-1*) showed a zygote-lethal phenotype, suggesting that RH27 may also function in biological processes beyond miRNA biogenesis. This possibility is supported by the additive effects observed in genetic analysis of *rh27-2*, *hyl1-2*, and *se-1* single and double mutants.

Mutation of *DCL1*, *HYL1*, or *SE* often results in reduced accumulation of miRNAs and increased levels of pri-miRNAs (Kurihara et al., 2006; Lobbes et al., 2006). However, in a genome-wide analysis of the *se-2* mutant, although a large subset of miRNAs (71%) showed reduced accumulation, the levels of a small proportion (8%) were increased (Wang et al., 2018). Similar results were observed in this study: the levels of a large subset of miRNAs (39% in shoots, 57% in roots) were reduced in the shoot apices and root tips of the *rh27-2* mutant, and the levels of a smaller proportion of miRNAs (29% in shoots, 23% in roots) were increased. Notably, we also observed reduced accumulations of pri-miRNAs in *rh27-2* shoot apices and root tips, as reported previously for the *ddl-1* mutant (Yu et al., 2008). We hypothesize that feedback regulation at the levels of miRNA transcription and processing may affect individual miRNAs and pri-miRNAs differently, as proposed before (Tang et al.,

2012; Feng et al., 2020). Alternatively, since RH27 is a member of a family of 58 DEAD-box RNA helicases in *Arabidopsis* (Mingam et al., 2004), the observed changes in the levels of a subset of miRNAs in the *rh27-2* mutant may represent only a fraction of the full complement of cellular miRNA biogenesis. Of course, with data obtained so far, we cannot exclude the possibility that RH27 may involve directly in miRNA transcription and stability.

Materials and methods

Plant materials and growth conditions

The *Arabidopsis* (*Arabidopsis thaliana*) ecotype Col-0 was used as the wild-type, and unless otherwise described, all mutants were in the Col-0 background. The *zyg4-1* (*rh27-1*) mutant was obtained by screening an ethyl methanesulfonate-mutagenized population, generated as described previously (Guo et al., 2016). The *rh27-2* mutant (SALK_068661) was obtained from the *Arabidopsis* Biological Resources Center (<https://abrc.osu.edu/>). The mutant lines *se-1* (Prigge and Wagner, 2001) and *hyl1-2* (SALK_064863; Vazquez et al., 2004), and the reporter lines *ProWOX5:erGFP* (Blilou et al., 2005), *QC25* (Sabatini et al., 2003), *ProCLV3:GUS* (Fletcher et al., 1999), *ProWUS:GUS* (Mayer et al., 1998), and *pEC1:H2B-RFP* (Ingouff et al., 2009) have been described previously. Plants were grown in commercially available humus soil at 21°C ± 2°C under a 16-h light (100 μmol photons m⁻² s⁻¹; supplied by white-light LED tubes) and 8-h dark cycle (Song et al., 2012). For seedling and RAM analyses, the surface-sterilized seeds were germinated on solid half-strength Murashige and Skoog (1/2 MS) salt medium containing 1% Suc and 1% agar and were vertically cultured. For SAM analyses, the seeds were germinated and cultured in liquid 1/2 MS medium on a rolling bank (Song et al., 2013).

Genetic analyses and molecular cloning

The *rh27-1/+* and *rh27-2* mutants were backcrossed to Col-0 for five and three generations, respectively, before further analyses. Map-based cloning of the mutation site in *rh27-1* was performed in 2,700 F₂ progenies from a cross between *rh27-1/+* and Landsberg *erecta* (*Ler*). A G-to-A point mutation was detected in a *rh27-1/+* plant after sequencing candidate genes. For complementation and expression analyses, the 2,227-bp 5'-upstream and the 2,914-bp genomic region (without the stop codon) of *RH27* was fused to the *GUS* or *sYFP* reporter gene of the *pPLV15* or *pPLV18* vector (De Rybel et al., 2011) using a one-step cloning method (Gibson et al., 2009). The obtained *ProRH27:RH27-GUS* and *ProRH27:RH27-sYFP* constructs were transformed into wild-type plants using the *Agrobacterium tumefaciens*-floral dip method (Clough and Bent, 1998). The *ProRH27:ΔRH27-sYFP* construct was generated by inserting the 2,227-bp 5'-upstream and truncated 2,604-bp genomic region (*ΔRH27*, a 310-bp deletion from start codon onward) of *RH27* into the *pPLV18* vector, as described above. All primers used are listed in Supplemental Data Set S2.

Microscopic and histological analyses

Whole-mount clearing and observation of ovules, shoot apices, and root tips (Yu et al., 2012), GUS assays (Song et al., 2013), and Lugol staining (Zhou et al., 2010) were performed as described previously. For histological analyses after GUS assays, shoot apices were embedded in Technovit 7100 (Heraeus Kulzer), and 5 μm sections were cut on a Leica microtome (Leica EM UC7). The sections were stained with periodic acid-Schiff's reagent (Baum, 2008) and photographed using a differential interference contrast-equipped microscope (Nikon 80i). The sizes (area) of the L1 cells in the SAM were measured and analyzed using ImageJ software (Schindelin et al., 2012). Transgenic plants carrying the fluorescent-reporter genes were examined under a Leica TCS SP5 or Zeiss LSM980 confocal laser scanning microscope. GFP was excited using a 488-nm laser line; sYFP was excited using a 514-nm laser line; and RFP was excited using a 561-nm laser line.

Reverse transcription quantitative PCR analyses

For RT-qPCR-based detection of pri-miRNAs and target genes of miRNAs, total RNAs were extracted from shoot apices and root tips (~ 5 mm) of seedlings at 5 DAG using the RNAprep Pure Plant Kit (DP432, Tiangen). For shoot apices collection, cotyledons, the first pair of leaves, hypocotyls, and roots were cut off using a razor blade under a dissecting microscope. Reverse transcription was performed using the FastQuant RT Kit (KR106, Tiangen) and qPCR was performed with iQ SYBRGreen Supermix (1708886, BioRad) on the BioRad CFX96 system, using *EIF4A* as a normalization control. For quantification of mature miRNAs, small RNAs were extracted from shoot apices and root tips (~ 5 mm) of seedlings at 5 DAG, collected as mentioned above, using the miRcute miRNA Isolation Kit (DP501, Tiangen), and reverse transcription was performed with the miRcute Plus miRNA First-Strand cDNA Kit (KR211, Tiangen). The qPCR analyses were performed with the miRcute Plus miRNA qPCR Kit (FP411, Tiangen) on the BioRad CFX96 system, using 5.8S rRNA or U6 snRNA as normalization controls. All data were analyzed using the $2^{-\Delta\Delta C_T}$ method (Livak and Schmittgen, 2001). The primers used are listed in Supplemental Data Set S2.

RNA in situ hybridization

In situ hybridization analyses of miRNAs were performed according to the method described by Javelle and Timmermans (2012), with 3'-end digoxigenin-labeled LNA modified probes (Supplemental Data Set S2). Antisense miR164 and miR124 probes were used at a final concentration of 50 nM and hybridized at 42°C overnight. The mRNA in situ hybridization analyses were conducted as described previously (Xin et al., 2017). For RNA probes, a 568-bp *CUC2* fragment was amplified from genomic DNA using gene-specific primers (Supplemental Data Set S2) and cloned into the *pEASY Blunt3* vector. PCR products containing the T7 promoter sequence, amplified from recombinant plasmids,

were used as templates for in vitro transcription. Slides were photographed under a bright field microscope (Nikon 80i).

RIP-RT-PCR

RIP-RT-PCR was performed as described previously (Ren et al., 2012). Briefly, wild-type seedlings at 10 DAG (approximately 2 g) were irradiated twice at 400 mJ/cm² in ice-cold PBS buffer. The nuclei were then extracted and lysed, and the cross-linked RNA–protein complexes were immunoprecipitated using a rabbit polyclonal anti-RH27 antibody, which was generated against His-tagged full-length RH27 and then purified by protein G using affinity chromatography. Three percent immunoprecipitates were analyzed by immunoblotting and detected using a mouse anti-RH27 polyclonal serum (1:3,000) generated against the same recombinant RH27 protein as that used to generate the rabbit anti-RH27 antibody. RNAs were then purified from RH27–RNA complexes with acidic phenol:chloroform:isopentanol (25:24:1), precipitated with 100% ethanol, and then digested with DNase I (M0303, NEB). Reverse transcription was performed using the First Strand cDNA Synthesis Kit with random primers (FSK101, TOYOBO). RT-PCR analyses were then performed using the primers listed in Supplemental Data Set S2.

Small RNA-seq and data analysis

Three sets of shoot apices and root tips (~ 3 mm) were harvested from wild-type and *rh27-2* seedlings at 5 DAG, as described for the RT-qPCR analyses. Approximately 30 mg were collected for each sample and total RNAs were extracted from the samples using the miRNeasy Mini Kit (217004, Qiagen). To prepare libraries, small RNAs were enriched from 2 μg of total RNAs using PEG8000, following the standard protocol (Berry Genomics). The libraries were pooled and sequenced on the Illumina Nextseq CN500 platform. For each small RNA-seq library, the sequences of the 3'-adaptors were removed and reads with sizes of 18–42 nt were selected using cutadapt (1.18; Martin, 2011). All clean reads were aligned to the Arabidopsis genome (TAIR10) using Bowtie2 (2.2.9; Langmead and Salzberg, 2012) with default parameters, and then alignments with up to one mismatch were selected. Reads were then aligned to the mature miRNA sequences from miRBase v22 using NCBI blast (2.2.26) with perfect matches. The aligned miRNAs were normalized against total mapped reads number of each library to calculate the reads per 30 million (RP30M) value. The Pearson correlation coefficient (r) of miRNA abundance was used to evaluate the consistency of replicate libraries. All replicate data sets were highly consistent ($r > 0.95$, P -value $< 10^{-100}$). Subsequently, miRNAs with a fold change > 1.5 were determined as differentially expressed.

RNA-seq and data analysis

Sample collections were performed as described for small RNA-seq. Total RNAs were extracted from the samples using the RNAprep Pure Plant Kit (DP432, Tiangen) and RNA

libraries were prepared following the standard protocol (Berry Genomics). The libraries were pooled and sequenced on the Illumina Nextseq CN500 platform. RNA-seq reads containing a 3'-adaptor sequence were discarded using cutadapt (1.18; Martin, 2011). All clean reads were then aligned to the Arabidopsis genome (TAIR10) using HISAT2 (2.1.0; Kim et al., 2015) with default parameters. Reads with a unique genome location were used for subsequent analyses. The numbers of reads mapped to a single gene annotated in Araport11 were counted using htseq-count script from HTSeq (0.6.0; Anders et al., 2015). The expression level of each gene was normalized by FPKM (Fragment count Per Kilobase of exon per Million fragments mapped) and codes to analyze the data are available at GitHub (<https://github.com/oneleaf425/rh27>). Differentially expressed genes were detected using R package edgeR (Robinson et al., 2010). Genes with a false discovery rate value less than 0.01 and fold change greater than 2 were regarded as differentially expressed. To analyze pri-miRNA levels, 325 pri-miRNAs annotated in Araport11 were acquired and counted using htseq-count separately to avoid overlapping with protein coding genes (Wang et al., 2019c). A total of 131 previously validated miRNA-target pairs were used to analyze the expression of miRNA target genes (Ma et al., 2018).

BiFC and LCI assays

For BiFC assays, the coding sequence of *RH27* was amplified from Arabidopsis and cloned in-frame to the coding sequence for the C-terminal region of YFP (cYFP) of the *pSPYCE-35S* vector. *SE*, *DDL*, *HYL1*, *DCL1*, or *AGO1* was cloned in-frame to the coding sequence for the N-terminal region of YFP (nYFP) of the *pSPYNE-35S* vector (Walter et al., 2004). The cYFP- and nYFP-fusion constructs were transformed into *A. tumefaciens* and pair-wise combinations were co-infiltrated into *Nicotiana benthamiana* leaves. After incubation for 24 h in the dark, followed by an additional 16 h light/8 h dark photoperiod, YFP signals were detected as described in Microscopic and Histological Analyses. Three independent assays were performed. Primers used for the constructs are listed in Supplemental Data Set S2.

For LCI analyses, the coding sequence of *RH27* was in-frame fused to the coding sequence for the N-terminus of nLUC in the *pCAMBIA1300-nLUC* vector, and the coding sequence of *SE*, *DDL*, *HYL1*, *DCL1*, or *AGO1* was in-frame fused to the coding sequence for the C-terminus of cLUC in the *pCAMBIA1300-cLUC* vector. The nLUC- and cLUC-fused constructs were transformed into *A. tumefaciens* and co-infiltrated pair-wisely into the leaves of *N. benthamiana*. LUC signals were detected under a low-light cooled CCD camera (Tanon) (Chen et al., 2008). Three independent assays were performed, and at least three leaves were co-infiltrated for each combination per assay. The primers used for the constructs are listed in Supplemental Data Set S2.

Co-immunoprecipitation assay

The cDNA sequence of *RH27* was cloned and fused in-frame to the coding sequence for the N-terminus of a Flag tag,

and the cDNA sequences of *SE*, *DDL*, *HYL1*, *DCL1*, and *NAC81* were cloned and fused to the coding sequence for the N-terminus of the Myc tag by introducing into the *pSuper1300* vector (Ni et al., 1995; Liu et al., 2017) to create the *RH27-Flag*, *SE-Myc*, *DDL-Myc*, *HYL1-Myc*, *DCL1-Myc*, and *NAC81-Myc* constructs. The primers used for the constructs are listed in Supplemental Data Set S2. *A. tumefaciens* strains carrying *RH27-Flag* were co-infiltrated pair-wisely with strains carrying the *SE-Myc*, *DDL-Myc*, *HYL1-Myc*, *DCL1-Myc*, or *NAC81-Myc* into 3-week-old *N. benthamiana* leaves. Leaf samples were collected after incubation for 24 h in the dark, followed by an additional 16 h light/8 h dark photoperiod, and were ground into a fine powder with liquid nitrogen. The leaf powder (0.5 g) was lysed with 1 mL NP-40 buffer (E124-01, GenStar) and incubated with anti-Myc beads (M047-11, MBL) according to the manufacturer's instructions. The anti-Myc bead-bound proteins were washed three times with NP-40 and analyzed by immunoblotting using anti-Myc (C3956, Sigma, lot 016M4762V, 1:3,000) or anti-Flag (M185-7, MBL, lot 004, 1:3,000) antibodies.

In vitro pull-down assay

The coding sequence of *DCL1*, *SE*, *HYL1*, or *DDL* was in-frame fused with the coding sequence for the C-terminus of GST in the *pGEX-6P-1* vector, and His-tagged *RH27* was generated in the *pET28SUMO* vector. The GST-fusion constructs were then transformed into *Escherichia coli* strain BL21 (DE3), and expression of the recombinant proteins was induced by incubation with 0.2 mM isopropyl- β -D-thiogalactoside at 20°C overnight. GST-tagged proteins were purified by affinity chromatography with Glutathione Resin (L00206, GenScript), according to the manufacturer's instructions. The *RH27-His* construct was transformed into the *E. coli* strain BL21 codon-plus RIL, and expression of the fusion protein was induced by incubation with 0.1 mM isopropyl- β -D-thiogalactoside at 16°C overnight. The induced cells were collected by centrifugation and lysed by sonication in binding buffer (20 mM Tris-HCl pH 8.0, 500 mM NaCl, and 25 mM imidazole). Subsequently, the clarified lysate was incubated with the prepared ProfinityTM IMAC Resins (156-0123, BioRad) at 4°C for 30 min. After washing the resin five times with binding buffer, the *RH27-His* protein was eluted with elution buffer (20 mM Tris-HCl pH 8.0, 500 mM NaCl, and 500 mM imidazole). GST protein pull-down assays were based on Glutathione MagBeads instructions (L00327, GenScript). Briefly, a 30- μ g sample of the GST, GST-DCL1, GST-SE, GST-HYL1, or GST-DDL fusion protein was incubated with Glutathione MagBeads. After washing out the non-bound GST-fused proteins, a 5- μ g sample of *RH27-His* was incubated with the beads bound by the GST-fused protein in 0.5 mL pull-down buffer (10 mM HEPES pH 7.5, 100 mM NaCl, 1 mM EDTA, 10% glycerol, and 1% Triton X-100) for 1 h at 4°C with intermittent shaking. The beads were then washed three times with pull-down buffer and collected for detection by immunoblotting with an anti-His antibody (D291-7, MBL, lot 008, 1:3,000). The

primers used for the constructs are listed in [Supplemental Data Set S2](#).

Accession Numbers

Sequence data from this article can be found in the Arabidopsis Genome Initiative or GenBank/EMBL databases under the following accession numbers: *RH27* (At5g65900), *WOX5* (At3g11260), *CLV3* (At2g27250), *WUS* (At2g17950), *HAM1* (At2g45160), *CUC1* (At3g15170), *CUC2* (At5g53950), *NAC100* (At5g61430), *PHB* (At2g34710), *PHV* (At1g30490), *CNA* (At1g52150), *REV* (At5g60690), *DCL1* (At1g01040), *SE* (At2g27100), *HYL1* (At1g09700), *DDL* (At3g20550), *AGO1* (At1g48410), *NAC81* (AT5G08790), and *EIF4A* (At1g54270). The protein sequences of *RH27* and its homologs in other species can be found in the National Center for Biotechnology Information (NCBI) database (www.ncbi.nlm.nih.gov/) under the following accession numbers: NP_201391 (*RH27*, *Arabidopsis*), BAS86908 (*OsRH27*, *Oryza sativa*), NP_080136 (*MmDDX18*, *Mus musculus*), CAG33341 (*HsDDX18*, *Homo sapiens*), Q03532 (*HAS1*, *Saccharomyces cerevisiae*), and NP_415318 (*RHLE*, *E. coli*). The small RNA and RNA-seq data sets described in this study have been deposited in the GEO database under accession number GSE154473.

Supplemental data

The following materials are available in the online version of this article.

Supplemental Figure S1. Alignment of *RH27* and its homologs, showing conserved motifs (supports [Figure 1, C](#)).

Supplemental Figure S2. Genotypic analyses of *zyg4-1* (*rh27-1*); *ProRH27:RH27-GUS* and *zyg4-1* (*rh27-1*); *ProRH27:ΔRH27-sYFP* seedlings (supports [Figure 1, D](#)).

Supplemental Figure S3. Abnormal seeds produced in *rh27-2/+* siliques (supports [Figure 1, A](#)).

Supplemental Figure S4. The expression of *ProWOX5:erGFP* in wild-type and *rh27-2* RAMs at 1, 3, 5, and 7 DAG (supports [Figure 2, E](#)).

Supplemental Figure S5. Altered SAM morphology and *ProCLV3:GUS* expression in *rh27-2* seedlings (supports [Figure 3, A](#)).

Supplemental Figure S6. The expression patterns of *ProWUS:GUS* in SAMs of wild type and *rh27-2* (supports [Figure 3, D](#)).

Supplemental Figure S7. Complementation of the *rh27-2* mutant by *ProRH27:RH27-sYFP* and expression analysis of the transgenic plants (supports [Figure 4](#)).

Supplemental Figure S8. The expression of *ProRH27:RH27-GUS* in seedlings and the inflorescence (supports [Figure 4](#)).

Supplemental Figure S9. In situ hybridization analyses of *CUC2* in wild-type (WT) and *rh27-2* shoot apices (supports [Figure 5, D](#)).

Supplemental Figure S10. Hierarchical clustering analysis showing the degree of reproducibility among different small RNA-seq libraries constructed for each genotype (supports [Figure 5, E and F](#)).

Supplemental Figure S11. Expression levels of miRNA target genes in shoot apices and root tips, as determined by RNA-seq analyses (supports [Figure 5, E and F](#)).

Supplemental Figure S12. Expression levels of pri-miRNAs in shoot apices and root tips (supports [Figure 6, A](#)).

Supplemental Data Set S1. Levels of miRNAs in shoot apices and root tips.

Supplemental Data Set S2. Sequences of the primers and probes used in this study.

Acknowledgments

The authors thank Dolf Weijers (Wageningen University) for sharing the *pPLV* vectors; Jian-Min Zhou (Institute of Genetics and Developmental Biology, Chinese Academy of Sciences) for the LCI vectors; Chongyi Xu (Institute of Botany, Chinese Academy of Sciences) for the *NAC81-Myc* construct; Shuxin Zhang (Shandong Agricultural University), Jin-Xin Liu (Institute of Botany, Chinese Academy of Sciences), Sheng-Yang Wu (Institute of Botany, Chinese Academy of Sciences), and Lei Guo (University of Maryland) for reading the manuscript and giving useful suggestions; Wei Xin (Institute of Botany, Chinese Academy of Sciences) for positive control probes and embedded blocks of RNA in situ hybridization; and Jingquan Li (Plant Science Facility of the Institute of Botany, Chinese Academy of Sciences) for technical assistance with the confocal laser scanning microscope.

Funding

This work was supported by the National Transgenic Science and Technology Program (grant no. 2019ZX08010-003), the National Natural Science Foundation of China (grant nos. 31871455, 30625016 and 31788103), and the Youth Innovation Promotion Association of the Chinese Academy of Sciences.

Conflict of interest statement. None declared.

References

- Anders S, Pyl PT, Huber W (2015) HTSeq—a Python framework to work with high-throughput sequencing data. *Bioinformatics* **31**: 166–169
- Andreuzza S, Li J, Guitton AE, Faure JE, Casanova S, Park JS, Choi Y, Chen Z, Berger F (2010) DNA LIGASE I exerts a maternal effect on seed development in *Arabidopsis thaliana*. *Development* **137**: 73–81
- Aubourg S, Kreis M, Lecharny A (1999) The DEAD box RNA helicase family in *Arabidopsis thaliana*. *Nucleic Acids Res* **27**: 628–636
- Autran D, Baroux C, Raissig MT, Lenormand T, Wittig M, Grob S, Steimer A, Barann M, Klostermeier UC, Leblanc O, et al. (2011) Maternal epigenetic pathways control parental contributions to *Arabidopsis* early embryogenesis. *Cell* **145**: 707–719
- Baum S (2008) The PAS reaction for staining cell walls. *CSH Protoc* **3**: 1–3
- Bliou I, Xu J, Wildwater M, Willemsen V, Paponov I, Friml J, Heidstra R, Aida M, Palme K, Scheres B (2005) The PIN auxin efflux facilitator network controls growth and patterning in *Arabidopsis* roots. *Nature* **433**: 39–44

- Botlagunta M, Vesuna F, Mironchik Y, Raman A, Lisok A, Winnard P, Jr, Mukadam S, Van Diest P, Chen JH, Farabaugh P, et al. (2008) Oncogenic role of DDX3 in breast cancer biogenesis. *Oncogene* **27**: 3912–3922
- Brand U, Fletcher JC, Hobe M, Meyerowitz EM, Simon R (2000) Dependence of stem cell fate in Arabidopsis on a feedback loop regulated by CLV3 activity. *Science* **289**: 617–619
- Cai W, Xiong Chen Z, Rane G, Satendra Singh S, Choo Z, Wang C, Yuan Y, Zea Tan T, Arfuso F, Yap CT, et al. (2017) Wanted DEAD/H or alive: helicases winding up in cancers. *J Natl Cancer Inst* **109**: 1–15
- Carlsbecker A, Lee JY, Roberts CJ, Dettmer J, Lehesranta S, Zhou J, Lindgren O, Moreno-Risueno MA, Vatén A, Thitamadee S, et al. (2010) Cell signalling by microRNA165/6 directs gene dose-dependent root cell fate. *Nature* **465**: 316–321
- Casamitjana-Martínez E, Hofhuis HF, Xu J, Liu CM, Heidstra R, Scheres B (2003) Root-specific *CLE19* overexpression and the *sol1/2* suppressors implicate a CLV-like pathway in the control of Arabidopsis root meristem maintenance. *Curr Biol* **13**: 1435–1441
- Chen H, Zou Y, Shang Y, Lin H, Wang Y, Cai R, Tang X, Zhou JM (2008) Firefly luciferase complementation imaging assay for protein–protein interactions in plants. *Plant Physiol* **146**: 368–376
- Clough SJ, Bent AF (1998) Floral dip: a simplified method for *Agrobacterium*-mediated transformation of *Arabidopsis thaliana*. *Plant J* **16**: 735–743
- De Rybel B, van den Berg W, Lokerse A, Liao CY, van Mourik H, Möller B, Peris CL, Weijers D (2011) A versatile set of ligation-independent cloning vectors for functional studies in plants. *Plant Physiol* **156**: 1292–1299
- Del Toro-De León G, García-Aguilar M, Gillmor CS (2014) Non-equivalent contributions of maternal and paternal genomes to early plant embryogenesis. *Nature* **514**: 624–627
- Dolan L, Janmaat K, Willemsen V, Linstead P, Poethig S, Roberts K, Scheres B (1993) Cellular organisation of the *Arabidopsis thaliana* root. *Development* **119**: 71–84
- Dong Z, Han M-H, Fedoroff N (2008) The RNA-binding proteins HYL1 and SE promote accurate *in vitro* processing of pri-miRNA by DCL1. *Proc Natl Acad Sci U S A* **105**: 9970–9975
- Fang Y, Spector DL (2007) Identification of nuclear dicing bodies containing proteins for microRNA biogenesis in living Arabidopsis plants. *Curr Biol* **17**: 818–823
- Feng Y, Yu Y, Zhou Y, Yang Y, Lei M, Lian J, He H, Zhang Y, Huang W, Chen Y (2020) A natural variant of miR397 mediates a feedback loop in circadian rhythm. *Plant Physiol* **182**: 204–214
- Fletcher JC, Brand U, Running MP, Simon R, Meyerowitz EM (1999) Signaling of cell fate decisions by *CLAVATA3* in Arabidopsis shoot meristems. *Science* **283**: 1911–1914
- Gibson DG, Young L, Chuang RY, Venter JC, Hutchison CA, III, Smith HO (2009) Enzymatic assembly of DNA molecules up to several hundred kilobases. *Nat Methods* **6**: 343–345
- Gong ZZ, Dong CH, Lee H, Zhu JH, Xiong LM, Gong DM, Stevenson B, Zhu JK (2005) A DEAD box RNA helicase is essential for mRNA export and important for development and stress responses in Arabidopsis. *Plant Cell* **17**: 256–267
- Gregory RI, Yan KP, Amuthan G, Chendrimada T, Doratotaj B, Cooch N, Shiekhattar R (2004) The microprocessor complex mediates the genesis of microRNAs. *Nature* **432**: 235–240
- Grishok A, Pasquinelli AE, Conte D, Li N, Parrish S, Ha I, Baillie DL, Fire A, Ruvkun G, Mello CC (2001) Genes and mechanisms related to RNA interference regulate expression of the small temporal RNAs that control *C. elegans* developmental timing. *Cell* **106**: 23–34
- Guan Q, Wu J, Zhang Y, Jiang C, Liu R, Chai C, Zhu J (2013) A DEAD box RNA helicase is critical for pre-mRNA splicing, cold-responsive gene regulation, and cold tolerance in Arabidopsis. *Plant Cell* **25**: 342–356
- Guo L, Jiang L, Zhang Y, Lu XL, Xie Q, Weijers D, Liu CM (2016) The anaphase-promoting complex initiates zygote division in Arabidopsis through degradation of cyclin B1. *Plant J* **86**: 161–174
- Han C, Liu Y, Wan G, Choi HJ, Zhao L, Ivan C, He X, Sood AK, Zhang X, Lu X (2014) The RNA-binding protein DDX1 promotes primary microRNA maturation and inhibits ovarian tumor progression. *Cell Rep* **8**: 1447–1460
- Ingouff M, Sakata T, Li J, Sprunck S, Dresselhaus T, Berger F (2009) The two male gametes share equal ability to fertilize the egg cell in *Arabidopsis thaliana*. *Curr Biol* **19**: R19–R20
- Ishida T, Aida M, Takada S, Tasaka M (2000) Involvement of *CUP-SHAPED COTYLEDON* genes in gynoecium and ovule development in *Arabidopsis thaliana*. *Plant Cell Physiol* **41**: 60–67
- Javelle M, Timmermans MCP (2012) In situ localization of small RNAs in plants by using LNA probes. *Nat Protoc* **7**: 533–541
- Khan A, Garbelli A, Grossi S, Florentin A, Batelli G, Acuna T, Zolla G, Kaye Y, Paul LK, Zhu JK, et al. (2014) The Arabidopsis STRESS RESPONSE SUPPRESSOR DEAD-box RNA helicases are nucleolar- and chromocenter-localized proteins that undergo stress-mediated relocalization and are involved in epigenetic gene silencing. *Plant J* **79**: 28–43
- Knauer S, Holt Anna L, Rubio-Somoza I, Tucker Elise J, Hinze A, Pisch M, Javelle M, Timmermans Marja C, Tucker Matthew R, Laux T (2013) A protodermal miR394 signal defines a region of stem cell competence in the Arabidopsis shoot meristem. *Dev Cell* **24**: 125–132
- Kim D, Langmead B, Salzberg SL (2015) HISAT: a fast spliced aligner with low memory requirements. *Nat Methods* **12**: 357–360
- Kinoshita A, Betsuyaku S, Osakabe Y, Mizuno S, Nagawa S, Stahl Y, Simon R, Yamaguchi-Shinozaki K, Fukuda H, Sawa S (2010) RPK2 is an essential receptor-like kinase that transmits the CLV3 signal in Arabidopsis. *Development* **137**: 3911–3920
- Kurihara Y, Takashi Y, Watanabe Y (2006) The interaction between DCL1 and HYL1 is important for efficient and precise processing of pri-miRNA in plant microRNA biogenesis. *RNA* **12**: 206–212
- Langmead B, Salzberg SL (2012) Fast gapped-read alignment with Bowtie 2. *Nature Methods* **9**: 357–359
- Laufs P, Peaucelle A, Morin H, Traas J (2004) MicroRNA regulation of the CUC genes is required for boundary size control in Arabidopsis meristems. *Development* **131**: 4311–4322
- Li HJ, Liu NY, Shi DQ, Liu J, Yang WC (2010) YAO is a nucleolar WD40-repeat protein critical for embryogenesis and gametogenesis in Arabidopsis. *BMC Plant Biol* **10**: 169
- Li S, Castillo-González C, Yu B, Zhang X (2017) The functions of plant small RNAs in development and in stress responses. *Plant J* **90**: 654–670
- Lin Z, Yin K, Zhu D, Chen Z, Gu H, Qu LJ (2007) AtCDC5 regulates the G2 to M transition of the cell cycle and is critical for the function of Arabidopsis shoot apical meristem. *Cell Res* **17**: 815–828
- Linder P, Jankowsky E (2011) From unwinding to clamping—the DEAD box RNA helicase family. *Nat Rev Mol Cell Biol* **12**: 505–516
- Liu M, Shi DQ, Yuan L, Liu J, Yang WC (2010) *SLOW WALKER3*, encoding a putative DEAD-box RNA helicase, is essential for female gametogenesis in Arabidopsis. *J Integr Plant Biol* **52**: 817–828
- Liu Z, Jia Y, Ding Y, Shi Y, Li Z, Guo Y, Gong Z, Yang S (2017) Plasma membrane CRPK1-mediated phosphorylation of 14-3-3 proteins induces their nuclear import to fine-tune CBF signaling during cold response. *Mol Cell* **66**: 117–128
- Livak KJ, Schmittgen TD (2001) Analysis of relative gene expression data using real-time quantitative PCR and the $2^{-\Delta\Delta C_T}$ method. *Methods* **25**: 402–408
- Llave C, Xie Z, Kasschau KD, Carrington JC (2002) Cleavage of *Scarecrow-like* mRNA targets directed by a class of Arabidopsis miRNA. *Science* **297**: 2053–2056
- Llobes D, Rallapalli G, Schmidt DD, Martin C, Clarke J (2006) SERRATE: a new player on the plant microRNA scene. *EMBO Rep* **7**: 1052–1058

- Ma X, Liu C, Gu L, Mo B, Cao X, Chen X** (2018) TarHunter, a tool for predicting conserved microRNA targets and target mimics in plants. *Bioinformatics* **34**: 1574–1576
- Mallory AC, Dugas DV, Bartel DP, Bartel B** (2004a) MicroRNA regulation of NAC-domain targets is required for proper formation and separation of adjacent embryonic, vegetative, and floral organs. *Curr Biol* **14**: 1035–1046
- Mallory AC, Reinhart BJ, Jones-Rhoades MW, Tang GL, Zamore PD, Barton MK, Bartel DP** (2004b) MicroRNA control of *PHABULOSA* in leaf development: importance of pairing to the microRNA 5'-region. *EMBO J* **23**: 3356–3364
- Martin M** (2011) Cutadapt removes adapter sequences from high-throughput sequencing reads. *EMBnet J* **17**: 10–12
- Mayer KF, Schoof H, Haecker A, Lenhard M, Jürgens G, Laux T** (1998) Role of *WUSCHEL* in regulating stem cell fate in the Arabidopsis shoot meristem. *Cell* **95**: 805–815
- Meyerowitz EM** (1997) Genetic control of cell division patterns in developing plants. *Cell* **88**: 299–308
- Mingam A, Toffano-Nioche C, Brunaud V, Boudet N, Kreis M, Lecharny A** (2004) DEAD-box RNA helicases in *Arabidopsis thaliana*: establishing a link between quantitative expression, gene structure and evolution of a family of genes. *Plant Biotechnol J* **2**: 401–415
- Müller R, Bleckmann A, Simon R** (2008) The receptor kinase CORYNE of Arabidopsis transmits the stem cell-limiting signal CLAVATA3 independently of CLAVATA1. *Plant Cell* **20**: 934–946
- Ngo QA, Baroux C, Guthörl D, Mozerov P, Collinge MA, Sundaresan V, Grossniklaus U** (2012) The Armadillo repeat gene *ZAK IXIK* promotes Arabidopsis early embryo and endosperm development through a distinctive gametophytic maternal effect. *Plant Cell* **24**: 4026–4043
- Ni M, Cui D, Einstein J, Narasimhulu S, Vergara CE, Gelvin SB** (1995) Strength and tissue specificity of chimeric promoters derived from the octopine and mannopine synthase genes. *Plant J* **7**: 661–676
- Nodine MD, Bartel DP** (2012) Maternal and paternal genomes contribute equally to the transcriptome of early plant embryos. *Nature* **482**: 94–97
- Paieri F, Tadini L, Manavski N, Kleine T, Ferrari R, Morandini P, Pesaresi P, Meurer J, Leister D** (2018) The DEAD-box RNA helicase RH50 is a 23S-4.5S rRNA maturation factor that functionally overlaps with the plastid signaling factor GUN1. *Plant Physiol* **176**: 634–648
- Palovaara J, de Zeeuw T, Weijers D** (2016) Tissue and organ initiation in the plant embryo: a first time for everything. *Annu Rev Cell Dev Biol* **32**: 47–75
- Prigge MJ, Wagner DR** (2001) The Arabidopsis *SERRATE* gene encodes a zinc-finger protein required for normal shoot development. *Plant Cell* **13**: 1263–1279
- Ren G, Xie M, Dou Y, Zhang S, Zhang C, Yu B** (2012) Regulation of miRNA abundance by RNA binding protein TOUGH in Arabidopsis. *Proc Natl Acad Sci U S A* **109**: 12817–12821
- Rhoades MW, Reinhart BJ, Lim LP, Burge CB, Bartel B, Bartel DP** (2002) Prediction of plant microRNA targets. *Cell* **110**: 513–520
- Robinson MD, McCarthy DJ, Smyth GK** (2010) edgeR: a bioconductor package for differential expression analysis of digital gene expression data. *Bioinformatics* **26**: 139–140
- Ronceret A, Gadea-Vacas J, Guillemot J, Lincker F, Delorme V, Lahmy S, Pelletier G, Chabouté ME, Devic M** (2008) The first zygotic division in Arabidopsis requires *de novo* transcription of thymidylate kinase. *Plant J* **53**: 776–789
- Sabatini S, Heidstra R, Wildwater M, Scheres B** (2003) SCARECROW is involved in positioning the stem cell niche in the Arabidopsis root meristem. *Genes Dev* **17**: 354–358
- Sarkar AK, Luijter M, Miyashima S, Lenhard M, Hashimoto T, Nakajima K, Scheres B, Heidstra R, Laux T** (2007) Conserved factors regulate signalling in *Arabidopsis thaliana* shoot and root stem cell organizers. *Nature* **446**: 811–814
- Schindelin J, Arganda-Carreras I, Frise E, Kaynig V, Longair M, Pietzsch T, Preibisch S, Rueden C, Saalfeld S, Schmid B, et al.** (2012) Fiji: an open-source platform for biological-image analysis. *Nat Methods* **9**: 676–682
- Schoof H, Lenhard M, Haecker A, Mayer KF, Jürgens G, Laux T** (2000) The stem cell population of Arabidopsis shoot meristems is maintained by a regulatory loop between the *CLAVATA* and *WUSCHEL* genes. *Cell* **100**: 635–644
- Schulz KN, Harrison MM** (2019) Mechanisms regulating zygotic genome activation. *Nat Rev Genet* **20**: 221–234
- Schüpbach T, Wieschaus E** (1986) Maternal-effect mutations altering the anterior–posterior pattern of the *Drosophila* embryo. *Roux Arch Dev Biol* **195**: 302–317
- Schwartz BW, Yeung EC, Meinke DW** (1994) Disruption of morphogenesis and transformation of the suspensor in abnormal suspensor mutants of Arabidopsis. *Development* **120**: 3235–3245
- Shen WH, Parmentier Y, Hellmann H, Lechner E, Dong A, Masson J, Granier F, Lepiniec L, Estelle M, Genschik P** (2002) Null mutation of *AtCUL1* causes arrest in early embryogenesis in Arabidopsis. *Mol Biol Cell* **13**: 1916–1928
- Shi R, Chiang VL** (2005) Facile means for quantifying microRNA expression by real-time PCR. *Biotechniques* **39**: 519–525
- Sieber P, Wellmer F, Gheyselinck J, Riechmann JL, Meyerowitz EM** (2007) Redundancy and specialization among plant microRNAs: role of the *MIR164* family in developmental robustness. *Development* **134**: 1051–1060
- Song L, Han M-H, Lesicka J, Fedoroff N** (2007) Arabidopsis primary microRNA processing proteins HYL1 and DCL1 define a nuclear body distinct from the Cajal body. *Proc Natl Acad Sci U S A* **104**: 5437–5442
- Song XF, Guo P, Ren SC, Xu TT, Liu CM** (2013) Antagonistic peptide technology for functional dissection of *CLV3/ESR* genes in Arabidopsis. *Plant Physiol* **161**: 1076–1085
- Song XF, Yu DL, Xu TT, Ren SC, Guo P, Liu CM** (2012) Contributions of individual amino acid residues to the endogenous *CLV3* function in shoot apical meristem maintenance in Arabidopsis. *Mol Plant* **5**: 515–523
- Stahl Y, Wink RH, Ingram GC, Simon R** (2009) A signaling module controlling the stem cell niche in Arabidopsis root meristems. *Curr Biol* **19**: 909–914
- Stahl Y, Grabowski S, Bleckmann A, Kühnemuth R, Weidtkamp-Peters S, Pinto Karine G, Kirschner Gwendolyn K, Schmid Julia B, Wink René H, Hülsewede A, et al.** (2013) Moderation of Arabidopsis root stemness by *CLAVATA1* and *ARABIDOPSIS CRINKLY4* receptor kinase complexes. *Curr Biol* **23**: 362–371
- Tang R, Li L, Zhu D, Hou D, Cao T, Gu H, Zhang J, Chen J, Zhang C-Y, Zen K** (2012) Mouse miRNA-709 directly regulates miRNA-15a/16-1 biogenesis at the posttranscriptional level in the nucleus: evidence for a microRNA hierarchy system. *Cell Res* **22**: 504–515
- Takada S, Hibara K-I, Ishida T, Tasaka M** (2001) The *CUP-SHAPED COTYLEDON1* gene of Arabidopsis regulates shoot apical meristem formation. *Development* **128**: 1127–1135
- Truernit E, Haseloff J** (2008) A simple way to identify non-viable cells within living plant tissue using confocal microscopy. *Plant Methods* **4**: 15
- van den Berg C, Willemsen V, Hendriks G, Weisbeek P, Scheres B** (1997) Short-range control of cell differentiation in the Arabidopsis root meristem. *Nature* **390**: 287–289
- Vazquez F, Gascioli V, Crété P, Vaucheret H** (2004) The nuclear dsRNA binding protein HYL1 is required for microRNA accumulation and plant development, but not posttranscriptional transgene silencing. *Curr Biol* **14**: 346–351
- Walter M, Chaban C, Schütze K, Batistic O, Weckermann K, Näke C, Blazevic D, Grefen C, Schumacher K, Oecking C, et al.** (2004) Visualization of protein interactions in living plant cells using bimolecular fluorescence complementation. *Plant J* **40**: 428–438

- Wang B, Chai H, Zhong Y, Shen Y, Yang W, Chen J, Xin Z, Shi H** (2019a) The DEAD-box RNA helicase SHI2 functions in repression of salt-inducible genes and regulation of cold-inducible gene splicing. *J Exp Bot* **71**: 1598–1613
- Wang D, Qin B, Li X, Tang D, Zhang Y, Cheng Z, Xue Y.** (2016) Nucleolar DEAD-box RNA helicase TOGR1 regulates thermotolerant growth as a pre-rRNA chaperone in rice. *PLoS Genet* **12**: e1005844
- Wang J, Mei J, Ren G** (2019b) Plant microRNAs: biogenesis, homeostasis, and degradation. *Front Plant Sci* **10**: 360
- Wang S, Quan L, Li S, You C, Zhang Y, Zhang Y, Gao L, Zeng L, Liu L, Qi Y, Mo B, Chen X** (2019c) The PROTEIN PHOSPHATASE4 complex promotes transcription and processing of primary microRNAs in Arabidopsis. *Plant Cell* **31**: 486–501
- Wang Z, Ma Z, Castillogonzalez C, Sun D, Li Y, Yu B, Zhao B, Li P, Zhang X** (2018) SWI2/SNF2 ATPase CHR2 remodels pri-miRNAs via Serrate to impede miRNA production. *Nature* **557**: 516–521
- Weigel D, Jürgens G** (2002) Stem cells that make stems. *Nature* **415**: 751–754
- Wu JJ, Peng XB, Li WW, He R, Xin HP, Sun MX** (2012) Mitochondrial GCD1 dysfunction reveals reciprocal cell-to-cell signaling during the maturation of Arabidopsis female gametes. *Dev Cell* **23**: 1043–1058
- Xin W, Wang Z, Liang Y, Wang Y, Hu Y** (2017) Dynamic expression reveals a two-step patterning of WUS and CLV3 during axillary shoot meristem formation in Arabidopsis. *J Plant Physiol* **214**: 1–6
- Xu J, Zhang HY, Xie CH, Xue HW, Dijkhuis P, Liu CM** (2005) *EMBRYONIC FACTOR 1* encodes an AMP deaminase and is essential for the zygote to embryo transition in Arabidopsis. *Plant J* **42**: 743–756
- Yang KJ, Guo L, Hou XL, Gong HQ, Liu CM** (2017) *ZYGOTE-ARREST 3* that encodes the tRNA ligase is essential for zygote division in Arabidopsis. *J Integr Plant Biol* **59**: 680–692
- Yin J, Park G, Lee JE, Choi EY, Park JY, Kim TH, Park N, Jin X, Jung JE, Shin D, et al.** (2015) DEAD-box RNA helicase DDX23 modulates glioma malignancy via elevating miR-21 biogenesis. *Brain* **138**: 2553–2570
- Yu B, Bi L, Zheng B, Ji L, Chevalier D, Agarwal M, Ramachandran V, Li W, Lagrange T, Walker JC, et al.** (2008) The FHA domain proteins DAWDLE in Arabidopsis and SNIP1 in humans act in small RNA biogenesis. *Proc Natl Acad Sci U S A* **105**: 10073–10078
- Yu D, Jiang L, Gong H, Liu CM** (2012) *EMBRYONIC FACTOR 19* encodes a pentatricopeptide repeat protein that is essential for the initiation of zygotic embryogenesis in Arabidopsis. *J Integr Plant Biol* **54**: 55–64
- Zhao L, Mao Y, Zhao Y, He Y** (2016) DDX3X promotes the biogenesis of a subset of miRNAs and the potential roles they played in cancer development. *Sci Rep* **6**: 32739
- Zhao P, Zhou X, Shen K, Liu Z, Cheng T, Liu D, Cheng Y, Peng X, Sun MX** (2019) Two-step maternal-to-zygotic transition with two-phase parental genome contributions. *Dev Cell* **49**: 882–893
- Zhou W, Wei L, Xu J, Zhai Q, Jiang H, Chen R, Chen Q, Sun J, Chu J, Zhu L, Liu CM, Li C** (2010) Arabidopsis tyrosylprotein sulfotransferase acts in the auxin/PLETHORA pathway in regulating postembryonic maintenance of the root stem cell niche. *Plant Cell* **22**: 3692–3709
- Zhou Y, Liu X, Engstrom EM, Nimchuk ZL, Pruneda-Paz JL, Tarr PT, Yan A, Kay SA, Meyerowitz EM** (2015) Control of plant stem cell function by conserved interacting transcriptional regulators. *Nature* **517**: 377–380
- Zhou Y, Yan A, Han H, Li T, Geng Y, Liu X, Meyerowitz EM** (2018) HAIRY MERISTEM with WUSCHEL confines *CLAVATA3* expression to the outer apical meristem layers. *Science* **361**: 502–506
- Zhu M, Chen G, Dong T, Wang L, Zhang J, Zhao Z, Hu Z** (2015) *SIDEAD31*, a putative DEAD-box RNA helicase gene, regulates salt and drought tolerance and stress-related genes in tomato. *PLoS ONE* **10**: e0133849